STUDY OF BEHAVIOR OF RCC BEAMS USING OPTICAL SENSORS AND STRENGHTENING WITH GFRP

A thesis report submitted

In the partial fulfillment of the requirement for the award of the degree of

MASTERS OF ENGINEERING

IN

STRUCTURAL ENGINEERING

Submitted by

AKSHAY SHARMA

(ROLL NO. 801524003)

UNDER THE GUIDANCE OF

Dr. NAVEEN KWATRA
Professor and Head
Civil Engineering Department
Thapar University, Patiala

Dr. A.B. DANIE ROY
Assistant Professor
Civil Engineering Department
Thapar University, Patiala

2017

CIVIL ENGINEERING DEPARTMENT

THAPAR UNIVERSITY, PATIALA – 147 004

PUNJAB, INDIA

DECLARATION

I, hereby declare that the thesis report entitled **"STUDY OF BEHAVIOR OF RCC BEAMS USING OPTICAL SENSORS AND STRENGHTENING WITH GFRP"**, submitted as per partial fulfillment of the requirements for degree of Masters of Engineering in Structural Engineering under the Department of Civil Engineering, Thapar University, Patiala is my own work under the guidance of Dr. Naveen Kwatra, (Professor and Head, Civil Engineering Department) and Dr. A.B. Danie Roy (Assistant Professor, Civil Engineering Department) during the academic year 2016-17. I confirm that the library may lend of copy of this upon request for academic purposes.

Dated: 31 / 07 / 2017

Akshay Sharma

Akshay Sharma,

801524003

CERTIFICATE

This is to certify that the work presented in thesis entitled **"STUDY OF BEHAVIOR OF RCC BEAMS USING OPTICAL SENSORS AND STRENGHTENING WITH GFRP"**, submitted by Akshay Sharma, Roll No. 801524003 is an authentic record of work carried out by the student under my guidance.

Dr. Naveen Kwatra
Professor and Head
Civil Engineering Department
Thapar University, Patiala

Dr. A.B. Danie Roy
Assistant Professor
Civil Engineering Department
Thapar University, Patiala

ACKNOWLEDGEMENT

I wish to express my deepest gratitude to Dr. Naveen Kwatra (Professor and Head , Civil Engineering Department, Thapar University Patiala) & to Dr. A.B. Danie Roy (Assistant Professor , Civil Engineering Department, Thapar University Patiala).The doors to my supervisors office were always opened whenever I ran into a trouble spot or had a query related to my thesis. They gave me their valuable time and also steered me in the path to complete this thesis work. They were always there whenever I needed counseling or expert guidance.

I would like to take this opportunity to thank Thapar University for offering this thesis where I learnt a lot and this exercise of writing a report helped me in improving my technical writing skills.

Also, I would like to thank the Department's lab staff who supported me in my work. Gratitude is due for my seniors too, Mrs. Priya Goyal, Mr. Sunil Garhwal and other research scholars of my department motivated me to complete my work.

Finally, special thanks to my friend Mayank Gupta who helped me a lot during the testing of my beams and to my brother Ashish Sharma and family members for their cooperation and support for completing this thesis.

-AKSHAY SHARMA

ABSTRACT

The new advancements in technology lead to discovery of new things which are then tried and tested for replacing the older ones. Though optical fiber is not new to the world but its fruitful use in telecom industry attracted the researchers to use it in various other fields whether it may be bio-medical or civil. In civil the use of softwares and data acquisition devices has helped the civil engineers to monitor the health of the structures continuously. Though various techniques have evolved for each study, 'Fiber Bragg Grating' based fiber optical sensors have come up as a new area of interest. Their small size, flexibility, embeddablity make them the perfect candidate to be used in the health monitoring studies.

The main aim for doing health monitoring studies is to keep an eye on the heath of the structure by monitoring various parameters such that any kind of anomaly could be detected and rectified before it affects the structure. In this study the flexure behavior of beams is studied by firstly pre-damaging them upto a certain load and then strengthening them with the help of glass fiber reinforced polymer. After strengthening, the beams were tested and various deductions were made by doing the vibration monitoring and four–point bending flexure test on the beams. In the first chapter of this report basic introduction of SHM, FOS has been provided followed by a review of literature of past research works in second chapter. The third chapter explains about the material properties, casting of specimens, test setups, and the sensors used. Finally, in the last chapter the results obtained from different tests have been discussed and later on conclusions are drawn.

Key Words:- Flexure, Fiber optical sensors, Fiber Bragg Grating, Strengthening, Glass Fiber Reinforced Polymer.

TABLE OF CONTENTS

LIST OF FIGURES

LIST OF TABLES

LIST OF ABBREVATIONS USED

ACTM	Automatic Compression Testing Machine
AE	Acoustic Emission
C/C	Centre to centre
CFRP	Carbon Fiber Reinforced Polymer
CSG	Conventional Strain Gage
DA	Data Acquisition
DAS	Data Acquisition System
FBG	Fiber Bragg Gratings
FOBGS	Fiber Optic Bragg Grating Sensors
FOS	Fiber Optics Sensor
FRC	Fiber Reinforced Concrete
GFRP	Glass Fiber Reinforced Polymer
GPR	Ground Penetrating Radar
LVDT	Linearly Varying Displacement Transducers
NDE	Non- Destructive Evaluation
NDT	Non- Destructive Testing
OSG	Optical Strain Gauge
RC	Reinforced Concrete
RCC	Reinforced Cement Concrete
SHM	Structural Health Monitoring
WASHMS	Wind And Structural Health Monitoring System

CHAPTER-1

INTRODUCTION

1.1 General

The arrangement of interrelated elements of something complex arranged to plan or a pattern is a structure. It can be of naturally found objects such as chemical's structure or other biological organisms, or it can be manmade objects such as buildings, machines etc. Thus, any structure in civil engineering is conceived keeping in its mind its intended use, the materials available, cost and aesthetic considerations. So, damage to such structures causes tremendous economic loss as well as heavy loss of life.

In the most general terms 'damage' is defined as changes introduced into a system's material and/or geometric conditions (including changes to the boundary conditions and system connectivity), that adversely affect its current or future performance. In this definition is the concept that damage is not meaningful without a comparison between two different states of the system, one which is used to represent the undamaged state and other pre-damaged. To properly monitor civil structures, its condition, or serviceability, must be assessed. Many variables can be monitored and used for the assessment. So, the process of implementing a damage detection and characterization strategy of engineering structures is referred to as Structural Health monitoring (SHM).

The increasing age of structures and the absence of flawless measures for structural safety have been the key driving forces for monitoring the health of the structure from the start of its service period. Earlier a structure was tested for deterioration and loss of property only when indications for the damage were found on the surface of the structure. But till that time the damages extended to structures reliability in most of the cases and also lead them to off commission or even at the verge of collapse. Thus, there is a need of a system which can monitor the health of the structure. Now-a-days various techniques have made it possible to study the behavior of these structures and rather than doing destructive testing, non-destructive testing is being preferred. But before the

NDT is applied to a larger structure, testing is done on smaller specimen which is then verified by destructive testing on the smaller structures.

1.2 Structural Health Monitoring

Process of implementing a damage detection and characterization strategy for engineering structures is referred to as Structural Health monitoring (SHM). **Chung *et al.* (2008)** defined structural health monitoring as the continuous measurement of the important parameters under service conditions to find out harmful changes in a structure as well as to provide proper periodic maintenance to increase the operational life of the structure, the main objectives of SHM are:

- To keep a check on the changes/modifications to an existing structure.
- To check the behavior of the structure during when it's affected by external disasters and extreme events like earthquake, tornado, fire etc.
- To make assessment of health of the structure post the external events.
- To monitor the structure during demolition.
- To provide fatigue assessment.
- To monitor structures subjected to long- term movement or derogation of materials.
- To provide a feedback loop such that the future design based on experience can be improved.
- To help in creation of novel system of construction and also check the growth in maintenance needs.

Hence, as compared to earlier times of destructive testing, several non-destructive evaluation (NDE) tools are being developed, and are available for put to use for monitoring (of which most can be wirelessly connected) such as strain gauges, inclinometers, displacement transducers, accelerometers, temperature gauges, pressure transducers, peizometers and fiber optic devices. These devices are used to measure the quantities like: acceleration, temperature & climatic condition, curvature, displacements, load (static/ dynamic), strain, tilt/slope, scour or to detect material derogation by means of corrosion, cracking, chemical attacks etc and also to find the location of these anomalies.

1.2.1. Classification of SHM systems

SHM system has been classified into four different levels considering different situations such as:

- Level I methods comprise of those methods that can analyze and establish if damage has occurred or not.
- Level II methods are those methods that find out if damage has occurred or not and simultaneously the location of damage.
- Level III methods comprise those methods which estimate the severity of damage by finding and analyzing the damage at different locations.
- Level IV methods are the methods that not only analyze the severity of damage after knowing the location of damage but also calculate the impact of damage on the health of structure.

1.2.2. SHM Methodology

SHM works incorporating all fields of engineering viz; civil, mechanical, electrical and computer engineering etc. Fig.1.1 gives the schematic of the SHM system.

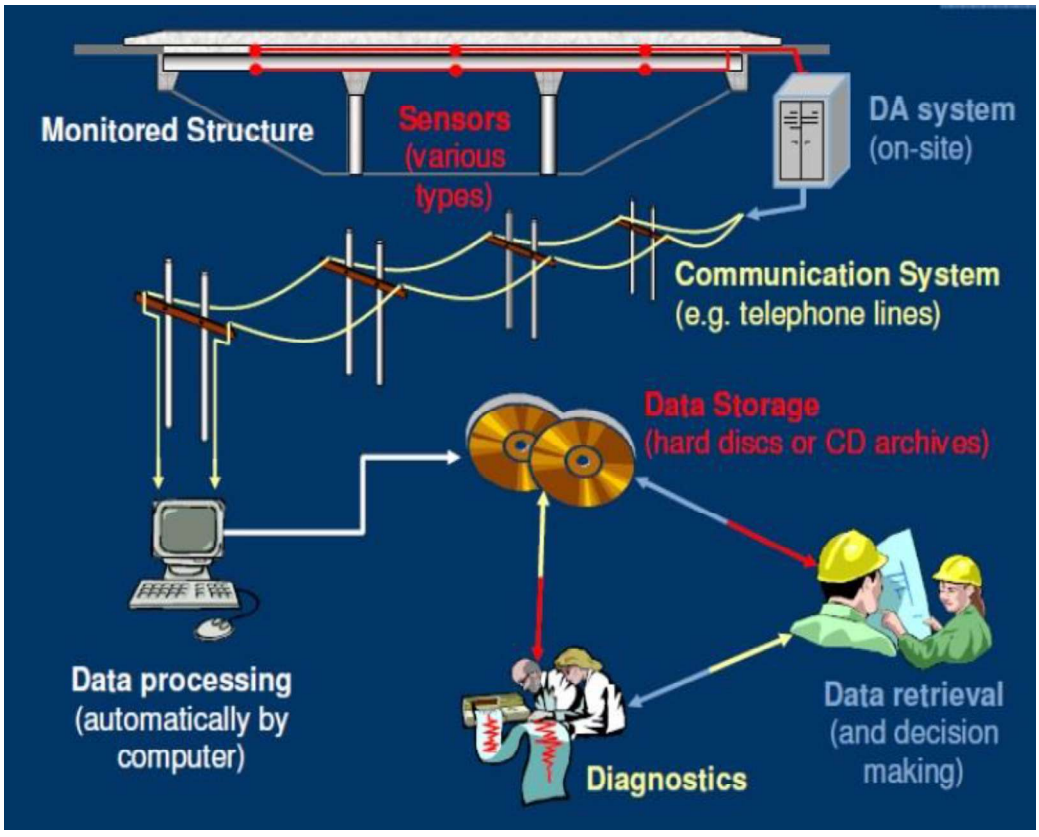

Fig.1. 1 Schematic of SHM components

From Fig.1.1, SHM has following components:

- Acquisition of Data

The raw data like accelerations, deflections, temperatures, loads, moisture levels etc. are acquired here. Data acquisition involves the following steps:-

- Selection of Sensors

The things to be taken care of while choosing a sensor are:-

  - Suitability for the task and robustness of sensors.
  - Time duration for which monitoring is to be done i.e. Long term vs. short term.
  - Particulars of the structure to be monitored.
  - Sensors serviceability conditions i.e., the sensors must serve desired purpose for the required duration.

- Sensor Installation and placement
  - The sensors should be installed without causing any hindrance in the behavior of the structure.
  - The supporting accessories such as sensor's wiring, junction boxes etc. must be included for initial structural design.
  - The construction should be according to the code.

- Transferring of data to data acquisition system (DAS)

Generally, there are two methods for transferring data to the DAS but the later one is being more followed these days:-

  - *Method-1*:- Direct physical link between sensors and DAS.

    It's the most common and least expensive. The drawback in this method is that, the long lead wires increase the "noise" in signals, thus making it difficult to use for large structures.
  - *Method-2*:- Wireless Transmission.

    This method is more expensive. In this the signals are transferred more slowly and less securely. But, if these two issues are resolved use of this method is expected to increase in the future

- Data Sampling and Collection

During data sampling and collection care should be taken that the quantity of data should neither be so scanty nor it should be so voluminous because if data is scanty it may jeopardize its usefulness and if it is voluminous it may be difficult to handle or may overwhelm the interpretation. The other concerning

issues include number of sensors, data sampling rates and data sorting for onsite storage.

- Communication of Data

  This refers to the data transfer from the DAS to an offsite location. It allows for remote monitoring, eliminating the site visits. DAS connects to offsite location by telephone lines, internet servers or wireless technologies.

- Intelligent Processing of Data

  It is required before data can be stored for later interpretation and analysis. The goal is to remove mundane data, noise, thermal, or other unwanted effects to make interpretation.

- Storage of Processed Data

  For storage of data, enough memory should be available. Data files should be well documented so that when the data is retrieved it should be understandable. Also, while saving it should not get corrupted so that raw data can be disregarded and re-interpretation can be avoided.

- Diagnostics

  It's one the important components in which we convert abstract data signals into useful information about structural response and condition. In general there are no well defined rules for diagnostics. The diagnostics depend on the type of the SHM technique used, type and location of sensor, parameters to be evaluated etc.

- Data Retrieval

  When storing the data for retrieval significance of data and the confidence in analysis is considered.

1.2.3. What is monitored, how and why?

Under SHM a lot of parameters can be monitored. A few of them are discussed below:

- Load
  - Arrangement and significance of forces applied to a structure are investigated i.e. whether the load is dissipating as expected or how the loads are distributed?
  - The load related monitoring is done by installing load cells or inferred using strain gauge data.

- Deflection
  - Sudden disproportionate deformations may result in a need for rehabilitation or upgrade.
  - These are measured by various transducers.
- Strain
  - The amount of change in dimensions defines the strain in a structure i.e. strain depends upon the magnitude of deformation too.
  - Strain at a given location can be find out using strain gauges which can comprise of Fiber Optic based strain gauge or electrical wire based strain gauge or vibrating wire strain gauge etc.
- Temperature
  - Variation in temperature due to thermal expansion or repeated loading cycles results in deformations in the structure.
  - Temperature also affects the strain readings so temperature effect must be eliminated from strain data.
  - Temperature is monitored using Temperature Controllers, TICs, thermostats, infrared thermography etc.
- Acceleration
  - Moving Loads/ Seismic Load etc. induces acceleration in structural components, thus leading to a question how is the structure resisting accelerations and the resulting loads?
  - That's why the accelerations are measured using accelerometers and is being extensively used in highly seismic regions.
- Wind Speed and Pressure
  - Wind load is the most important load while designing long span bridges and tall buildings. It lays the ground rules for the design of such structure
  - So, to record the speed and pressure at various locations, anemometers are being used.
- Acoustic Emission
  - The latest SHM technique in which the A.E. devices listens for noise variation i.e. when a certain structural component breaks, it will emit noise and using that noise the location of that crack is pin-pointed.
  - Microphones and various sound receptors can be used to do monitoring by acoustic emission.

- This technique is used in post-tensioned concrete and cable stayed structures.

- Video Monitoring
  - To find the root cause of the deformations, to correlate the data with the images video monitoring is done.
  - Time stamped videos and pictures can be used to witness maximum load events. Internet camera technology can be used for this purpose.

So, in short it is observed for monitoring of parameters like loads, deflections, strains, temperature etc. NDT techniques can be used. NDT is becoming a powerful investigative tool not only because of its ability to detect problems without inducing further damage, but also because it does so with minimal expenditures of time and manpower. Considering the potential gains associated with nondestructive testing, there is a significant lack of expertise available. Identifying the deterioration mechanisms and defects most relevant to structures is the first step. **Rehman Ur kashif S. *et al.* (2016)** and **McCann D.M. (2001)** have compared various NDT methods as summarized in Table 1.1 below.

Table 1. 1 Comparison of various non-destructive test methods used in SHM

Test name	Description	Application/ Capabilities	Limitations
Impact Echo	Seismic or Stress Wave based method	(1) Detects:- • Anomalies in concrete. • Delamination in Plain Cement concrete and reinforced concrete elements • Wave reflectors. • Overlay debonding. • Ducts. • Voids. (2)Surface opening cracks characterization. (3) Grouting characterization. (4) Concrete modulus of elasticity evaluation. (5) Concrete compressive strength estimation.	(1) This test detects concrete overlays only when the temperature of concrete is low. (2) Detections are possible only when the material is highly viscous. (3) Only loosely bonded overlay are detectable. (4)Interference of signals is prominent on limited dimensional elements like girders, piers etc. (5) For marking the boundaries of delimited area dense grids are required.

Test name	Description	Application/ Capabilities	Limitations
Ultra Sonic Pulse Velocity	Ultrasonic (acoustic) stress wave based method	(1) Detects:- • Debonding of steel bars. • Shallow cracking • Delamination • Grouting defects. • Material interface. (2)Assess faults in concrete. (3)Can be used to find the depth of elements.	(1) Its a time consuming method. (2)Data quality is strong only when the coupling of sensor unit is good. (3)Very close grid spacing is required in this method. (4) Shallow defects and some other defects may remain undetected due to use of lower frequencies.
Impulse Response	Also known as Transient dynamic or mechanical impedance method, extension of vibration test	(1) Detects:- • Cracks. • Honeycombing • Voids • Delamination in concrete. • Debonding of overlays. (2) Determine:- • Loss of support below rigid pavements. • Load transfer at joints of concrete pavements • Sub grade modulus. (3) This method is used as a screening tool for potential damage detection.	(1) Selection of test points is required for reliable data interpretation. (2) Smaller defects may remain undetected. (3) Automated apparatus is not available.
Acoustic Emission	Transient elastic waves	(1) Real-time damage detection. (2) Remote monitoring. (3) Applicable for both local and global monitoring. (4) Continuous monitoring without interrupting the traffic flow. (5) Reliable analysis.	(1) Background noise problem. (2) Difficult to apply analysis to real structure. (3) No standard procedure for all types of bridges.

Test name	Description	Application/ Capabilities	Limitations
Half-Cell Potential	Electrochemical method	(1) Active corrosion is determined. (2) It can be used at any time. (3) Climatic condition does not affect the reading.	(1) Min. temperature must be higher than $2^{o}C$. (2) Effect on concrete cover depth is still unknown. (3) Correcting data for depth is difficult. (4) It cannot be used for moisture or salt content calculation. (5) Cannot take reading on the isolating layer (6) Measurements are often unreliable.
Electrical Resistivity	Based on voltage and current measurement	(1) Detects:- • Moisture • Crack presence. (2) ER surveys can be used to map corrosion activity (3) Determine:- • Susceptibility of concrete towards corrosion. • Regions susceptible to chloride penetration.	(1) Raw data storage & interpretation is more challenging. (2) ER depends upon material properties like moisture content, salt content, porosity etc. (3) It is very difficult to find out the contribution of specific one in overall results. (4) Automated measurement is not available in market. (5) Surface has to be pre-wetted.
Infrared Thermography	Based on electromagnetic waves, infrared region, emitting from the surface of the material related to temperature variation	(1) Detects:- • Cracks. • Voids • Delamination in concrete. • Debonding • Change in density, thermal conductivity and specific heat capacity. • Segregation in asphalt concrete.	(1) Difficult to detect deep flaws. (2) Do not give data about depth of crack. (3) Surface irregularity, boundary condition and atmospheric temperature influence the results.

So, to get more data and better analysis as compared to the methods discussed above researchers are trying to find a new way to accomplish the monitoring by using fiber optic sensors which are more reliable and easy to use.

1.3 Fiber Optic Sensors

Many of the conventional sensors being used in the health monitoring aspects are based on the electric signal transmission. But their limitations are becoming more and more manifest. They are big in size, they are not durable enough to be embedded in a structure to measure the properties internally. They are local sensors, confined to measure properties at a single point and cannot be multiplexed easily. In some cases, noise is very high due to electrical and magnetic interferences which make a demodulating system necessary for these kinds of sensors. These all add up in increasing the problems of using the conventional sensors in SHM.

According to **Udd E. (1995)** past 30 years witnessed an immense increase in research in the field of optical fiber sensing. They're flexible, embeddable, multiplex-able and EMI immune. Optical fibers are usually made up of glass or plastic, the strand which has a diameter of that of a human hair. Compared to the copper wires, optical fibers are less expensive, thinner, have higher data carrying capacity, less signal degradation, carry digital signals and are non-flammable, lightweight and flexible. Since signals degrade less, lower power transmitters are used instead of the high-voltage electrical transmitters required for copper wires. The signal coming out of optical fiber wire posses the same quality and intensity as when it was first entered into the cable. An optical cable is resistant to electromagnetic interference, as well as to crosswalk from adjoining wires.

So, optical fibers can be used as sensors to measure strain, temperature, pressure and other parameters. The small size and the fact that no electrical power is needed at the remote location give the fiber optic sensor advantages to conventional electrical sensor in certain applications. Optical fiber sensors for temperature and pressure have been developed for down-hole measurement in oil wells. The fiber optic sensor is well suited for this environment as it is functioning at temperatures too high for semiconductor sensors (Distributed Temperature Sensing). Another use of the optical fiber as a sensor is the optical gyroscope which is in use in the Boeing 767 and in some car models (for navigation purposes) and the use in Hydrogen micro sensors.

1.3.1 Classification of fiber optic sensors

Madhikani M. *et al.* (2008) have classified fiber optic sensors into two major categories namely intension-metric and interfero-metric sensors. In intension-metric, sensor depends on change in the radiant power conducted through an optical fiber, while an interfero-metric sensor relies on induced phase change in light propagating through the optical fiber. Further, optical fiber sensors areof four types:-

- Fabry-Perot Sensors
- Long Gauge Sensors
- Brillouin Scattering Sensors
- Fiber Bragg Grating Sensors

1.3.1.1 Fabry-Perot Sensors

- In these sensors, optical fiber is cut and a "gap" is inserted because in this optical technique the change in gap width is determined and the quantity is measured.
- Highlighting features of fabry –perot sensors are:-
    - It can only be used to measure the local (point) strains.
    - Use for static and dynamic monitoring.
    - Cannot be multiplexed.
    - These are embeddable, bondable and weldable.

1.3.1.2 Long Gauge Sensors

- In these sensors, the sensor senses the path displacement in the gauge length. Gauge length is defines as the distance between mirrors. 'Low Coherence Interferometry' optical technique is used in these sensors.
- Characteristic features of long gauge sensors are:-
    - The gauge length varies from 5cm to 100m.
    - Can be used for static monitoring only.
    - Thermal compensation is also required in these sensors.
    - These sensors are highly versatile.

1.3.1.3 Brillouin Scattering Sensors

- Though these types of sensors are at developmental stage only but yet these are capable of measuring static strain profiles using a single optical fiber.
- Main features are:-
  - Till now these are capable of static monitoring only.
  - Through these sensors, thermal and mechanical strains can be separated.
  - These are currently, very expensive as extensive signal processing and analysis is required.

1.3.1.4 Fiber Bragg Grating (FBG) Sensors

- Most commonly used sensors which depend on the reflection of light from a region in the refractive index of the optical fiber core.
- According to **Rodrigues *et al.*(2010)**, FBG sensor acts as a selective wavelength filter that reflects just the spectral part satisfying the Bragg condition with the wavelength of the peak reflectivity, λ_b, expressed as ,

  $$\lambda_b = 2\, n_{eff}\, \Lambda \qquad \ldots\ldots\ldots(1)$$

  Where,

  n_{eff} is the effective refractive index of the fiber core at the free-space center wavelength.

  Λ is the grating period.

  A change in the period of grating or effective refractive index (can be caused by strain (and temperature) change) leads a shift of the Bragg wavelength. Thus, the reflected peak wavelength, when submitted to a strain variation, $\Delta\varepsilon$, and temperature variation ΔT, shifts by a magnitude of $\Delta\lambda_b$, which can be expressed as,

  $$\Delta\lambda_b = P_e\, \Delta\varepsilon + [\, P_e\, (\alpha_s - \alpha_f) + \zeta\,]\, \Delta T \qquad \ldots\ldots\ldots(2)$$

  Where,

  P_e is the strain optic coefficient.

  α_s and α_f are thermal expansion coefficients.

  ζ is the thermo- optic coefficient.

  The FBG sensor's interrogation is performed by optoelectronic equipment consisting essentially of a light source, a photo detector and optical couplers, all working together.
- Major Characteristics are

- These sensors, though used only for local point strains but can be serially multiplexed.
- These require temperature compensation but are embeddable, bondable and weldable.

1.3.2 Applications of fiber optic sensors

There are numerous ways by which fiber optic sensors can be put to use. Some of the few applications given **by Madhikani M. *et al.* (2008)** and Li **H. N. *et al*. (2004)** are discussed here as follows:

1.3.2.1 As stress sensors

Structural monitoring is concerned with the safety of the users of a structure, especially for the case of building structures and infrastructures. When considering the safety of a structure, the maximum stress in a member due to live load, earthquake, wind, or other unexpected loadings must be checked not to exceed the allowable stress of a member. In allowable stress design of steel structures, if the maximum stress in a member reached the yield stress, the member is considered to be analogous to failure. Therefore, to guarantee the safety of a structure and its users, the maximum stress in a member must be monitored. Since the actual stress distribution induced in a beam by varying amounts and types of loads is non-uniform, many difficulties exist when determining the maximum stress in a beam with the point sensors. In this case, the reliability of the evaluated safety depends on the number and location of point sensors. Various fiber optic systems based on different mechanisms have been developed to assess the safety of structural members.

1.3.2.2 As strain sensors

Strain sensors measure the relative displacement between two points in a structure. The distance between the two points along the fiber optic changes through various environmental effects. It is noticeable that due to the deformation measured is the average value measured, the strain variation or stress distribution of a beam can be considered by using several fiber optic sensors, and by means of these sensors the maximum strain or stress in a beam can be measured.

The strain sensors consist of a fiber Bragg grating sandwiched between layers of carbon composite material and are about 50 mm long and 0.5 mm thick. The accuracy and sensitivity of the sensors are dependent upon the optical system.

1.3.2.3 As temperature sensors

Thermal expansion is an important factor in all types of structures where differential heating may occur, either from environmental effects, such as the solar heating of pavements and bridge decks, or from service conditions, such as in nuclear-reactor, pressure vessels or furnaces. The thermal expansion coefficient will be a variable quantity depending on materials. The Bragg wavelength λ_B, is related to the grating period, Δ, and the effective refractive index of the fiber n_{eff} by $\lambda_B = 2\Delta n_{eff}$. Subjecting the fiber to a change of temperature causes Δn_{eff} and therefore λ to change. By determining the wavelength of reflectivity, the temperature to which the fiber is subjected may be found. Typically, the temperature sensor is packaged into a 35 mm long metal tube. The metal tubing protects the fiber Bragg grating from external stress and increases the temperature sensing range.

1.3.2.4 To crack monitoring

The existing condition of many important concrete structures can be accessed through the detection and monitoring of cracking. For example, in concrete bridge decks, crack openings beyond 0.15 to 0.2 mm will allow excessive penetration of water and chloride ions, leading to the corrosion of steel reinforcements. The crack opening of the order of millimeters, which may occur after a major earthquake, is a sign of severe structural damage.

Conventionally, crack detection and monitoring have been carried out by visual inspection. The procedure is time consuming, expensive, and yet unreliable. Recently, researchers developed sensors for the reliable detection and monitoring of cracks in concrete structure. An optical fiber is embedded in the concrete element in a ‘‘zigzag’’ shape and before the formation of cracks, the light intensity distribution along the fiber is measured. When a crack opens in the structure, fiber bend to stay continuous and consequently light intensity is changed.

1.3.2.5 To moisture monitoring

Due to the nature of concrete structures and their exposed environmental conditions, corrosion can occur internally without this being evident from the outside. This is often due to the ingress of water corroding the reinforcements, which is hastened by the salts and chloride ions dissolved in it. At the moment, fiber optic based humidity sensor has been developed and used for the measurement of moisture absorption in concrete. The sensor was fabricated using a fiber Bragg grating coated with a moisture sensitive polymer. The sensor itself exploits the inherent characteristics of the fiber Bragg grating. It was found that optical fiber based humidity sensors form a basis for determining the changes in the moisture content in different concrete samples, indicating new applications of the sensors to ensure the integrity of structures.

1.3.2.6 To welding residual stress monitoring

Optical fiber sensors due to their small size are becoming to be widely used in high electromagnetic fields. This feature is combined with excellent stability and also with the possibility of having several optical fibers. As result of their features, a kind of sensors constitutes a very powerful tool for the analysis of welding transient and residual stresses. Under the assumption of a perfect bonding between the plate and the sensor, we are actually measuring transient and residual strains in the material being welded. Optical fiber sensors have been already used to detect welding transient and residual stresses in several kinds of structures.

1.3.2.7 To buildings

The optical fiber sensing technology has been employed in safety condition monitoring of the high –rise structure during in-construction and in-service stages. **Li H.N. *et al.* (2004),** reported that in early 2001, four long gage Bragg grating sensors were installed across, above and under the primary arch of the Cathedral of Como in Northern Italy to identify any significant structural deterioration to protect this significant structural deterioration to protect this significant cultural heritage built in 1396. Four sensors were installed using surface mounting brackets. The sensor installed across the arch had a total gauge length of 7 m with a spring mechanism and the rest all have a gauge length of 100 mm. Each sensor has two serially connected Bragg gratings. One

grating measures strain, while the other monitors temperature. Displacement resolution of 0.1 μm and temperature resolution of 0.1^{o}C were achieved with the technique of fiber Fabry–Perot tunable filter demodulation system. The eight-month period measurement showed that the temperature was consistent with seasonal variation and the displacements were not substantial. Along with the high resolution of FOSs, the advantage of embeddability is often exploited in health monitoring. In general, FBG sensors are used to monitor the strain and temperature of any component of the building in three steps of construction, that is, before the concrete pouring, during the pouring and curing of concrete.

1.3.2.8 To piles

Piles are very important to support and protect buildings from shocks or earthquakes. The piles are tested for a three point bending test is performed to ensure the survivability of the FBGs and the insensitivity of the FBG temperature sensors to mechanical strain. Then driving tests and real-time monitoring is done to know if there is apparent bending existing in the pile. Compression and pull out tests can also be done to measure the strain and load eccentricity which can be helpful for health monitoring of piles.

Using FBG's young's modulus, vertical displacement and forces can be measured. In addition, properties of soil, critical strain when crack occurs in the pile, ultimate load capacity of a pile and failure mode in the interface of soil and pile can also be measured.

1.3.2.9 To pipelines

Not only can average strains be measured, but cracks can also be monitored by FOS. FOSs can also monitor cracks or accidents that occur in long pipelines. In Indonesia, a 110 km pipeline was equipped with a vibration sensor to monitor its integrity and to alert ongoing damages because of third party interference from excavation equipment, theft, and landslide or earth movement. Based on the principle of modal-metric interference effect, the vibration monitoring unit pinpoints the location of a normally by detecting the changes of back scattered light characteristics caused by disturbances of fiber compression, elongation or twist.

In October 1998, the system operator was alerted of a major event that caused damages to the pipeline at 46.81 km. Upon further inspection, it was discovered that a landslide had occurred and a section of 24-inch pipeline was fully exposed. This system can monitor a fiber of length up to 50 km with a resolution of 0.1 km. The monitoring technology demonstrated its unique potential in health monitoring of long pipelines since such accidents to pipelines could not be easily detected by other conventional methods. Moreover, new types of leakage detecting sensors are being developed to exploit this huge potential market. It is reported that several novel FBG based pressure, flow, and seismic sensors could be used in reservoir, oil and gas pipeline, and well-drilling applications.

1.3.2.10 To highway monitoring

FBG sensors have displayed many obvious advantages over traditional loop inductors, piezo-ceramic weigh-in-motion systems and regular vehicle monitoring devices because of its immunity to radio and electrical interference. In addition, the FBG sensors have the potential to act as road parameter sensor (humidity, ice, temperature, etc.) and they can be integrated into one FOS intelligent transportation system for infrastructure planning, traffic surveillance, traffic monitoring, and road tolls.

1.3.2.11 To bridges

Bridges, especially concrete bridges, are the most monitored civil structures by FOSs. The applications of fiber optic sensors to bridge monitoring are focused in measurement of short and long-term parameters of bridges. Successful implementations of long-term health monitoring systems on bridges have been widely reported. More than 40 long span bridges (with spans of 100m or longer) worldwide have been instrumented with structural health monitoring systems based on fiber optic sensors. Typical examples are the Great Belt Bridge in Denmark, the Confederation Bridge in Canada, the Tsing Ma Bridge in Hong kong, the Commodore Barry Bridge in United States, the Akashi Kaikyi Bridge in Japan and the Seohae Bridge in Korea.

All the tools/equipments for monitoring the health of a structure are used over bridges. Anemometers, Temperature sensors, Strain gauges, accelerometers, displacement transducers, global positioning systems, weigh-in-motion

systems, corrosion sensors, elasto-magnetic sensors, optic fiber sensors, tilt meters, level sensors, total stations, seismometers, barometers, hygrometers, pluviometers, video cameras a can be used to monitor each aspect of the bridge.

1.4 About the study

1.4.1 Objectives

The prime objectives of this work are:-

- To study the flexural of behavior of pre-damaged RCC beams strengthened by Glass fiber reinforced polymer (GFRP).
- To prove the effectiveness of the newly acknowledged FBG sensors over conventional sensors.
- To study the variation in health of beams before and after pre-damaging them and after the application of GFRP to them via vibration monitoring.

1.4.2 Flexure testing in R.C.C. beams

The design of R.C.C. beams is done keeping in mind the expected failure of beam. In general, two failures are defined for beam like structures namely, 'tension failure' and the 'compression failure'. The tension failure is that failure in which the amount of steel in RCC beams is kept less than the balanced section, such a beam is called the under-reinforced beam. In these beams the yielding of steel leads to crack formation in the structure, thus indicating future collapse of section and a sudden collapse of structure is avoided. While in case of compression failure, steel is kept higher with respect to that in the balanced section. The failure here is brittle one as the failure of concrete mass occurs. This failure happens suddenly without any warning signs thus this kind of failure should be avoided.

Though tension failure and compression are responsible for failing of RCC beams (on the basis of design) but there are two major failures in RCC beams that occur due to the type of loading and material property of the concrete. They are shear failure and flexure failure. A shear load is that type of load which tries to produce a sliding failure in the material along a plane that is parallel to the direction of force. For example, cutting of a paper is an example

of shear failure. Thus, shear strength is very important for deciding the dimensions of RCC beams, and the main purpose of reinforcing stirrups is to increase the shear strength of RCC beams.

While flexural strength is the material property, it is defined as the highest stress experienced by the beam its moment of yield in a flexure test. The transverse bending test is most frequently employed, in which a specimen having either a circular or rectangular cross-section is bent until fracture or yielding using a three point or four point flexural test techniques.

The flexural tests are conducted to determine the mechanical properties of resin and laminated fiber composite materials. Further, these tests are used to find the inter laminar shear strength of a laminate, shear modulus, shear strength, tensile and compression moduli along with the flexural and shear stiffness.

In this study, the RCC beam samples are subjected to four point flexural test. In this method the beam is loaded by two loads placed symmetrically between the supports. In this method there are four important points (two end supports and two loading points) along the span of the beam. Thus, it gives four-point bending.

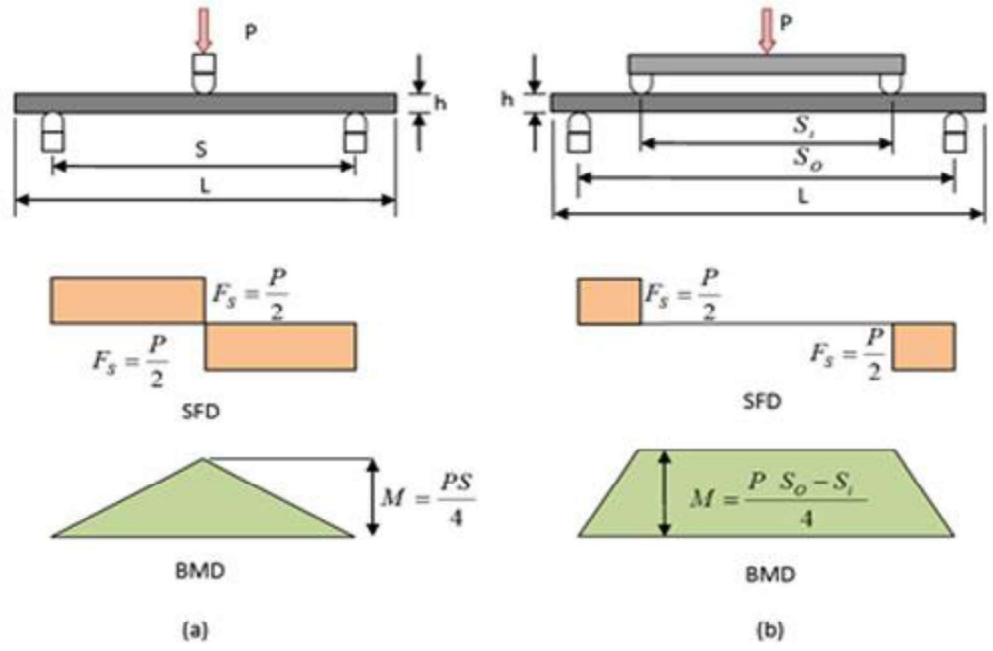

Fig.1. 2 Shear force diagram and Bending moment diagram for (a) 3-point load test (b) 4-point load test.

From the Shear force and bending moment diagrams in Fig.1.2 for 3-point and 4-point tests there is concentration at the point of loading. However, for 4-point test there is uniform bending moment and both shear force and inter-laminar shear stress are zero between the loading points. Thus, it leads to the pure bending loading. Such a condition of stress is desirable during testing.

1.4.3 Strengthening of R.C.C. beams

By structural strengthening the main aim is to restore / add up in the capacity of the structural elements. Primarily, it is expected that structural strengthening can increase the load capacity of beams, columns, walls, support additional live or dead load which were not included in original design, to relieve stresses exerted on the structural element by design or construction errors, or to restore the original load carrying capacity to damaged structural elements.

For strengthening purpose the most commonly used materials are like advanced composite material such as FRP (Fiber reinforced polymers) composites or structural steel plates.

FRP composites have been used in aerospace and manufacturing applications from a very long time. They are light in weight, have high tensile strength and non-corrosive structural properties. GFRP and CFRP are the most commonly used strengthening materials. In this study Glass fiber reinforced polymer has been used.

1.4.4 Vibration monitoring

The vibration mentioning's main purpose is to check for damage detection of structural elements. Many researchers found that if the new natural frequency obtained during a routine operation varies from that of the original natural frequency value, the building should be checked for possible local defects.

But in this study the main objective of doing vibration monitoring is to study how the application of GFRP to the pre-damaged beams brings variation to the vibration signature of the beams.

CHAPTER-2

LITERATURE REVIEW

2.1 General

Beams are the one of the basic elements of every structure. Without them we cannot imagine a structure to be as whole. They not only help in distributing the loads but increase the stiffness of the structure too. From a very long time beam's behavior study has been the one of the favorite subject for researchers to study. If any new technology is emerged its first tested on beams only. Some of these type of studies have been discussed here.

2.2 FBG in various structure studies

Before discussing the use of FOS let's discuss the work of researchers using other NDT techniques. **Clark M.R. *et. al* (2003)** worked with infrared thermography on concrete and masonry bridges. In their study they successfully showed how the infrared thermography is a better technique than visual technique as they found anomalies (delamination in concrete) in the bridge structure while the surface of the bridge was dry and showed no sign of any anomaly.

Rhazi Z. (2001) performed three tests on the McDonald Bridge deck (Montreal). Three tests used were infrared thermography, half cell potential technique and ground penetrating radar (GPR) technique. Half cell potential technique helped in inferring that corrosion had started but the corrosion had not been reached upto such an advance stage such that it may cause delamination. GPR failed to generate conclusive results as the wavelength of the radar in concrete was not able to detect the 1-2mm wide delamination cracks. Infrared thermography only indentified the areas where the delamination in concrete was happening.

Similarly, **Shiotani T. (2007)** used acoustic emission technique to monitor health of 45-m bridge span by passing 20 ton crane over the bridge three times with a constant speed of 0.5m/s. Here, dealmination areas were identified by means of quantification indices like calm ratio and I*b*-value. Later these areas of concrete delamination were confirmed by means of ultra sonic pulse velocity test.

After reviewing these literatures it can be inferred that though the new non-destructive tests are a good replacement for destructive testing and visual inspection but they leave a gap, like these sensors have to be affixed on the surface of the structure, continuous stream of data monitoring is not available with these NDT techniques i.e. no real time monitoring is there.

Study of health monitoring of Tsing Ma bridge was done by **Chan *et al.* (2005)**. The researchers tried to monitor strain in the various parts of the bridge and also compared the performance of FBG sensors with the conventional health monitoring system namely, WASHMS. Strain sensors, both conventional and FBG ones were put up at different locations and strain vs. time plots were drawn (Fig. 2.1 to Fig. 2.3).

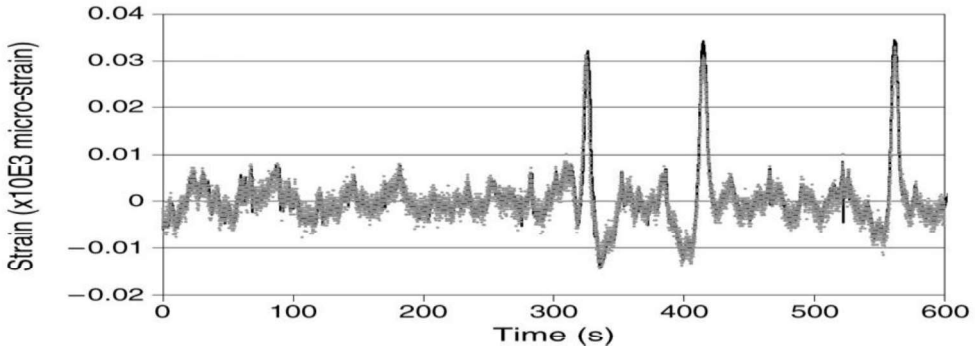

Fig. 2. 1 Comparison of Strain measured by FBG senors (Dot) and WASHMS strain gauge (line) when sensors were put below the deck of the bridge.(*Chan et. al* (2005)).

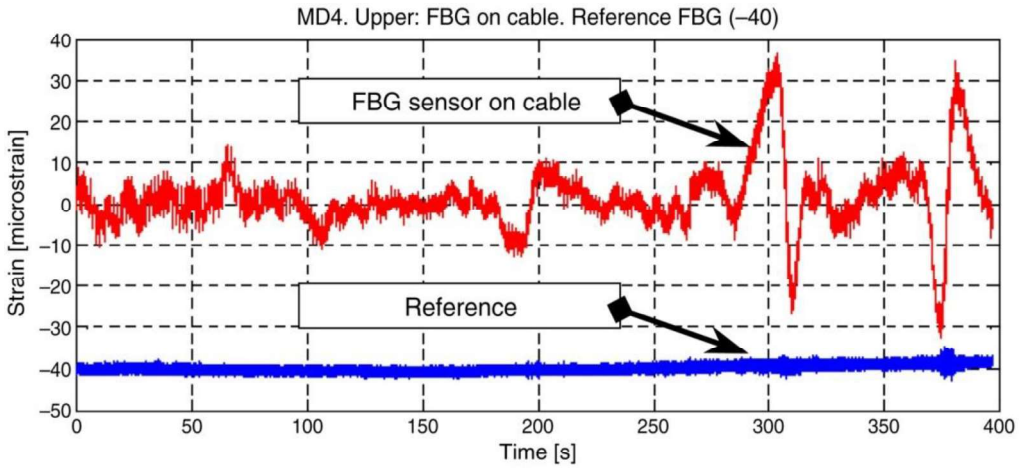

Fig. 2. 2 Hanger cable measurement history (Chan *et al.* (2005))

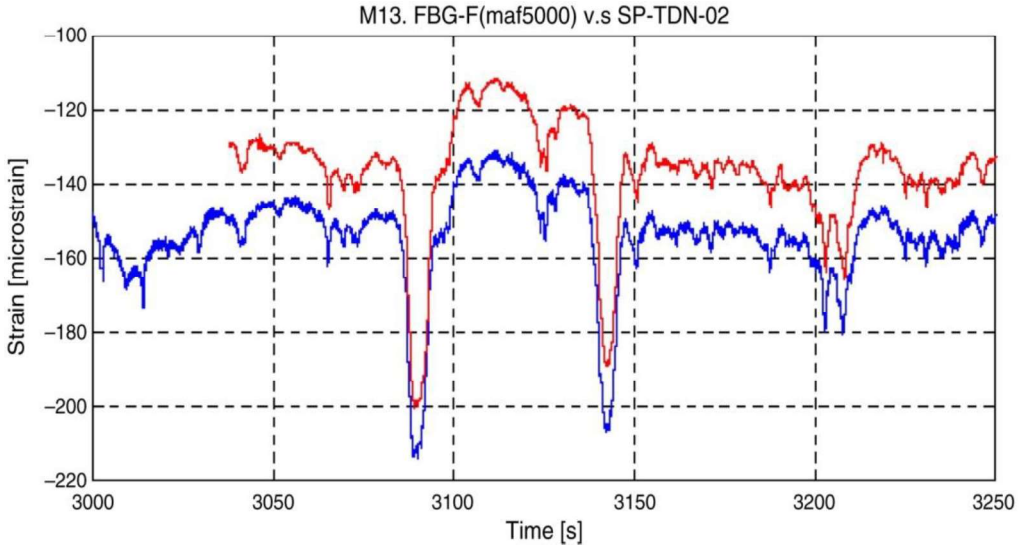

Fig. 2. 3 Comparison between FBG (upper) and conventional strain gauge (lower) histories after filtering data (Chan *et al.* (2005))

The three figures show the strain vs. time plots when the strain and the conventional sensors are put at different location of the bridge. The Fig.2.1 shows the strains measured by the sensors when three trains paased through the bridge at about 320, 420and 560s. Fig.2.2 records the passage of the trains at 307s and at 377s by the sensors mounted at hanger cable. Also in the middle of the graph, passage of high traffic can also be seen (corresponds to t=195s).Fig. 2.3 shows the strain time plot when sensors were mounted over rocker bearing during TMB construction.

So, it is evident from the three graphs FBG are as capable as any other conventional SHM system because the strain-time plots of FBG SHM system and WASHM system are in complete agreement of each other.

Kister G. *et al.* (2007) report use of Bragg grating sensors in foundation piling. Optical fiber sensors were used on two reinforcing cages. Appropriate protection systems for the sensors were developed. Two piles were chosen for the study and the detail of position of sensors is shown in fig.2.4. Of the two foundation piles only one pile was available for periodic monitoring as during construction the sensors in one of the pile were damaged due to some manual error. Bragg sensors were interrogated during the pouring and curing of the concrete and also during the construction of the different floors of the building. The following graphs were obtained during the whole monitoring process Fig.2.5 – Fig.2.8.

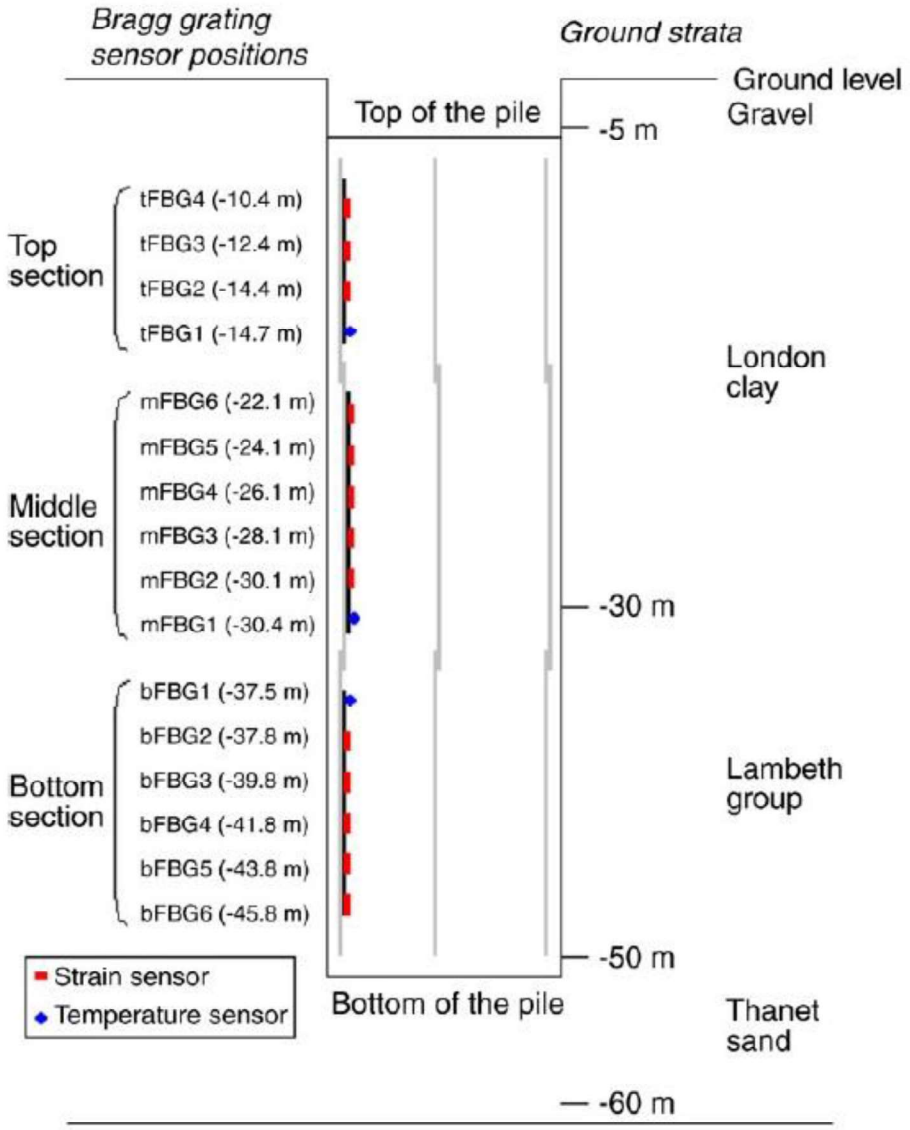

Fig. 2. 4 Ground composition and position of FBG sensors in foundation pile (Kister G. *et al.* (2007))

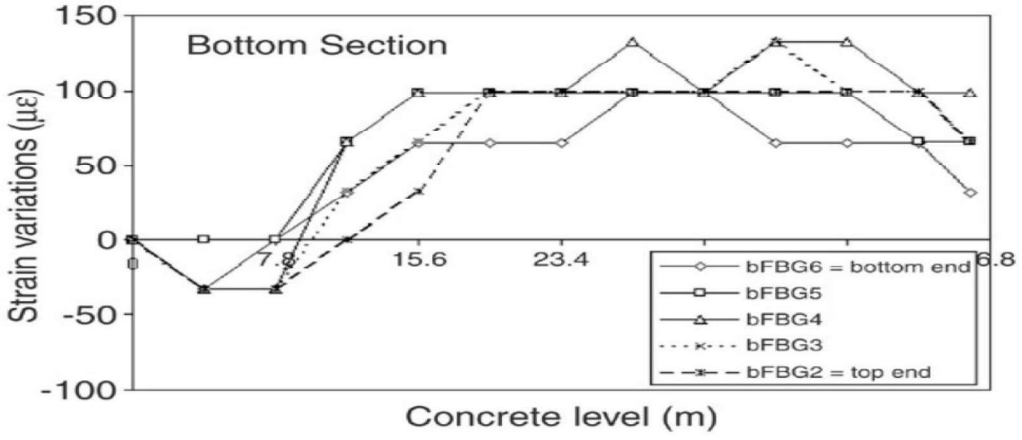

Fig. 2. 5 Strain variation in the bottom section of the cage during the concrete pouring (Kister G. *et al.* (2007))

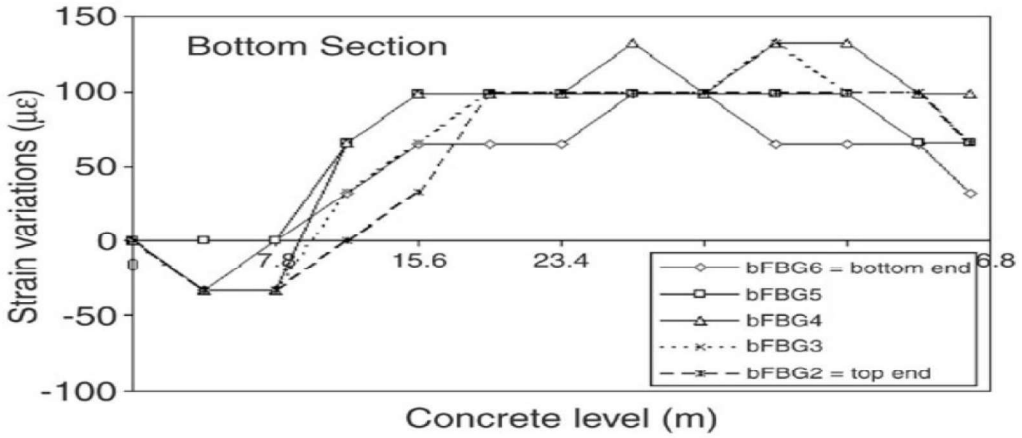

Fig. 2. 6 Strain variation in the middle section of the cage during concrete pouring (Kister G. *et al.* (2007))

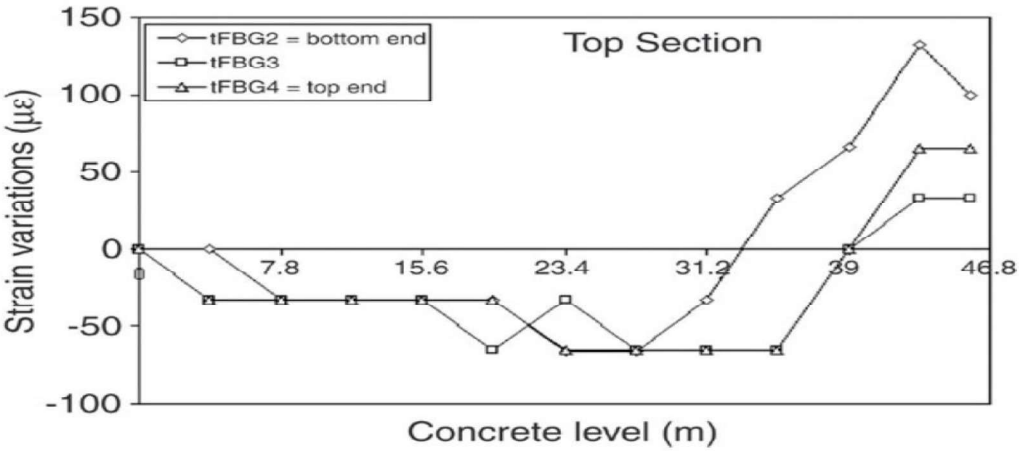

Fig. 2. 7 Strain variation in the top section of the cage during the concrete pouring (Kister G. *et al.* (2007))

With reference to above three figure compressive and tensile strains were measured. The transition of strains comes into play when the level of concrete reached an optical strain sensor. Also when the subsequent construction of different floors was done strain distribution with the whole depth of pile was observed. Decreasing tensile strains and increasing compressive strains were measured during the concrete curing in the cage sections. These strains were attributed due to the decreasing concrete temperature and the increasing weight of the concrete. After the 21st day, increasing compressive strains were recorded along the pile depth. This build-up of compressive strains was due to the final phase of the concrete curing, the construction of the different building floors and the ground heave from excavation.

Again similar study was carried out by **Costa *et al.* (2012)**. The monitoring system was to be implemented, “Luiz-I bridge”. For monitoring three types of sensors namely, strain, temperature and displacement sensors were to be used. Also, the study had to be a decade long study, in which the welding of sensors was not allowed. So, the three major issues to be addressed were, firstly, the monitoring was to be carried for a very long time so the sensor should not be affected by the environmental factors. Secondly, the sensors should be based on the same principle so that a single data acquisition system may suffice the purpose. Thirdly, they sensors should be lightweight and flexible as they had to be attached via some other source rather than welding. So, to fill the conditions, FBG based health monitoring system was chosen. For this the FBG sensors were tested by means of laboratory tests like static behavior test, fatigue testing, creep evaluation tests were conducted.

Strain- Time plot shown in Fig. 2.8 was obtained when bridge was initially tested for 15 minutes time interval. Because of passage of vehicles 6 postive peaks showing the maximum effect were generated on the slab considered, while the two negatives lobes with positive lobe was because of vehicles passing on the neighboring spans.

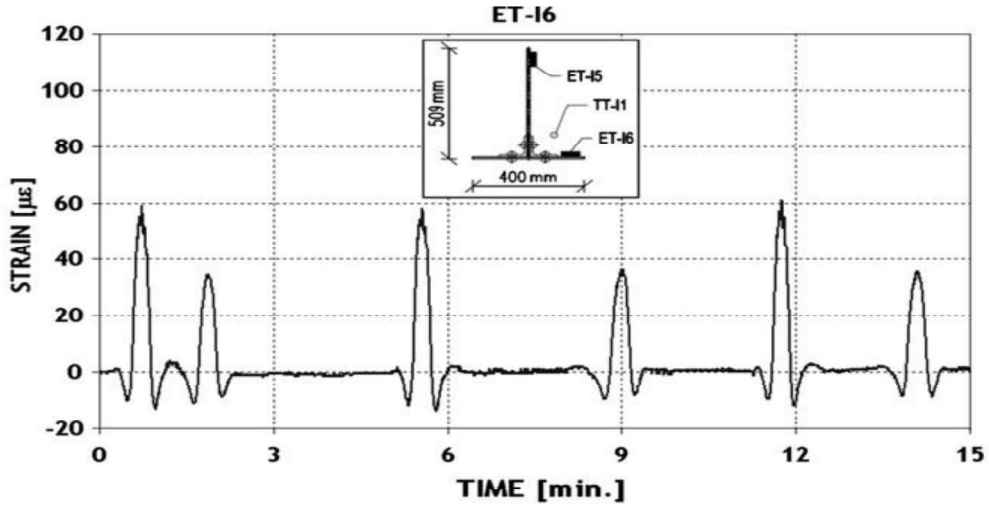

Fig. 2. 8 Fifteen- minute strain-time plot from the strain acquired by the strain sensor (Costa *et al.* (2012)

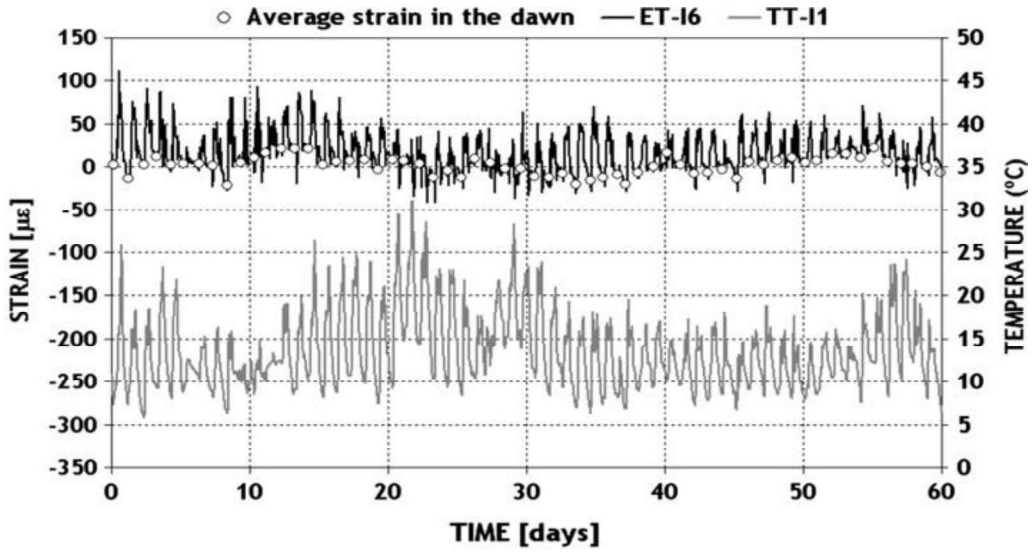

Fig. 2. 9 Results of strain and temperature sensors during the first two months of observation (Costa *et al.* (2012)).

From the Fig. 2.9, it is clear that the average strain is affected by the temperature. Also, they reported that no trend in measurement was found which could be related to strain sensor's creep.

From these three studies it can be concluded that FBG sensors are the perfect replacements for the conventional sensors, they are so much more flexible such that they can be used by embedding in concrete or pasted below the deck of bridge, they can work normally.

2.3 Fiber optic sensors application to beams

Uttamchandani *et al.* (1999) reported for RC structures fiber composite rebars, optical fiber sensor technology is best suited for load related studies because of flexible nature of optical fibers, they can be embedded with the rebars in the during fabrication. Thus, for uniaxial structures, optical fibers can easily fit into the composite material without any voids and can be entirely integrated with the structure.

Lau Kin-tak *et al.* (2001) presented a theoretical model to evaluate the differential strains between the bare fiber and host material with various adhesive thickness and modulus of protective coating of the embedded FBG sensor. The specialty of using FBG sensor for strain sensing application is that it is able to measure strains locally with high resolution and accuracy. The accuracy while

using the FBG strain sensors depends on the bonding characteristics of the fiber core, protective coating, adhesive layer and host material.

In this work, a theoretical model for the mechanical load transfer from the host material to the bare fiber is addressed by considering the adhesive material thickness. The results were then compared with numerical analysis using the finite element method (FEM). It was found from the theoretical analysis that short bonding lengths influence the final strain measurement at the fiber-optic grating region. The thick adhesive layer and low modulus of coating material with a short embedding length of sensor is not beneficial as for embedded FBG strain sensing systems the maximum shear stress and shear stress concentration region increase with increasing thickness of adhesive layer and decreasing modulus of coating material. Sufficient embedding length of the sensor is essential to avoid mis-measurement using FBG strain sensors.

A minimum embedding length was evaluated by using the following equation:-

$$L_f = \frac{1}{\lambda} \sin^{-1} h \left\{ \frac{1}{0.01} \sin h \left(\lambda L_g \right) \right\}$$

Where,

L_g represented the FBG sensor length.

L_f represented bonded length.

Kuang K.S.C. *et al.* (2003) examined the use of plastic optic fiber sensors for crack detection and vertical deflection monitoring in concrete beams. In the experiment, a series of scale-model concrete specimens and full-scale RC beams have been were tested under flexural loading conditions to evaluate the possibility of using low cost, POF sensors for detecting crack initiation, post-crack vertical deflection and failure in civil engineering structures. The POF sensor used to monitor flexural loads relied on the loss of light when the sensor was bent. The POF lost light to the environment through evanescent penetration and as a result of a significant reduction in the number of propagation modes that experience total internal reflection. In order to improve the sensitivity of the POF to vertical deflections and crack initiation, a segment of the POF cross sectional profile was cut over a predetermined length by abrading the surface of the POF using a razor blade.

The results of the three-point bend tests on the small concrete samples are shown in Fig. 2.10. Here, in specimens 1 and 2, loading was discontinued immediately after peak load. But for others to monitor the ability of the sensor to detect cracks, the remaining specimens were loaded beyond peak load to assess the sensor's ability to monitor vertical deflections in cracked samples. From the figure, it is evident that in each of the six specimens crack propagation at peak load is accompanied by a significant drop in the sensor response. In addition to showing the ability of the POF sensor to detect crack initiation, the results also highlighted the potential of the sensor to monitor the post-crack vertical deflection as evidenced by the high degree of linearity in the optical signal after peak load.

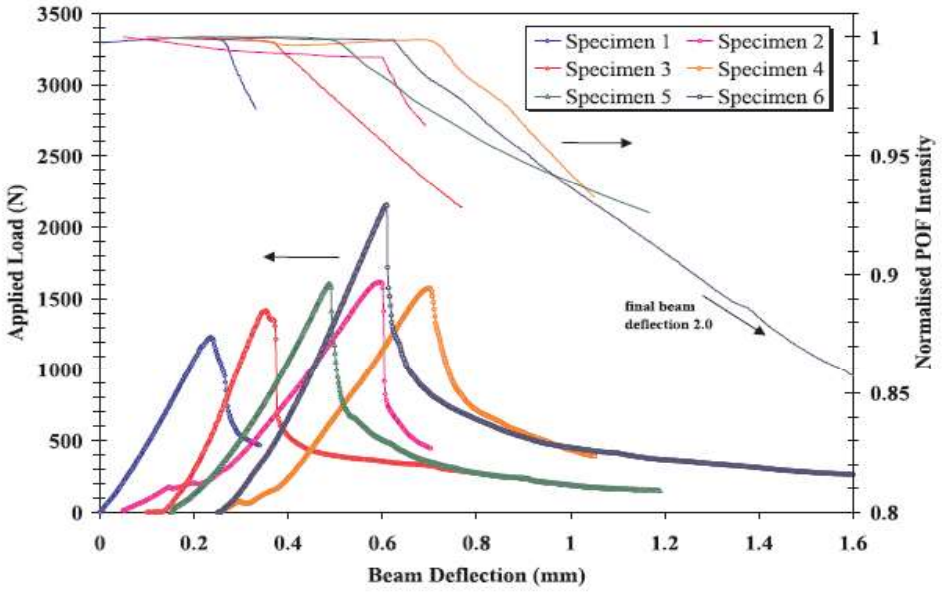

Fig. 2. 10 Three point bend test on the scale model concrete specimens. (Kaung K.S.C. *et al.* (2003))

In full scale reinforced concrete beam tests, the load was applied monotonically up to failure. In this test, only one sensor was used in specimen 1 attached to the lower surface of the beam and in specimen 2, a second sensor was attached to the side surface of the beam in addition to it. In these tests, the sensor response was analyzed and compared to the concrete load–deflection data. Fig. 2.11 shows the load– displacement curve and corresponding optical signal data from specimen 1. It can be seen from the plot that at the damage initiation and failure thresholds, an accompanying change in the sensor response is there. Also, after detecting the

initial crack, the sensor exhibits an almost linear response before failure of the concrete specimen occurs at a beam deflection. From the plot, it is clearly evident that an instantaneous reduction in signal intensity accompanies failure of the concrete beam. From Fig. 2.12 similar results for the second specimen can be seen, in which two sensors were employed simultaneously. Both sensors were able to detect the presence of an initial crack and subsequent failure of the beam. The sensor signal after initial cracking exhibits a high degree of linearity, again highlighting the sensor's ability to monitor crack propagation in these concrete structures.

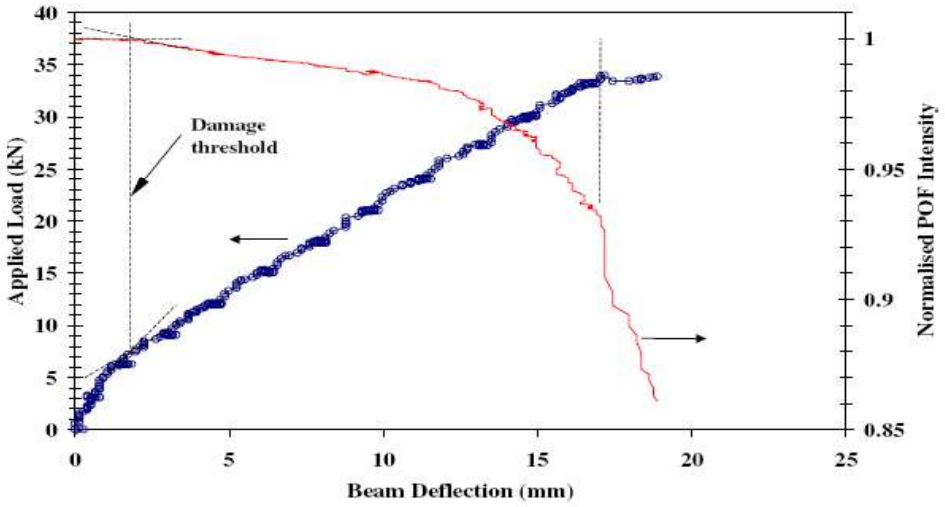

Fig. 2. 11 Sensors response during three-point bend tests on a full scale RC beam. (Kaung K.S.C. *et al.* (2003))

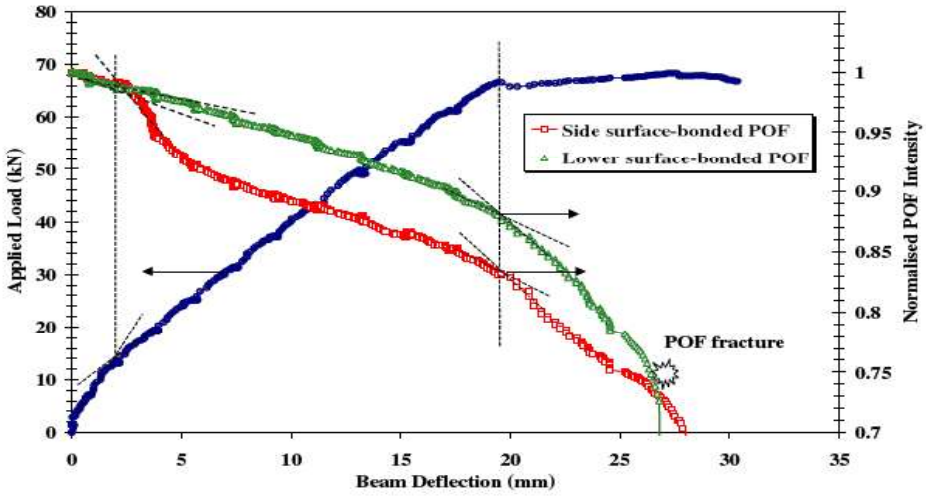

Fig. 2. 12 Response of side and lower surface mounted sensors during three point bend tests on a full scale RC beam. (Kaung K.S.C. *et al.* (2003))

From the results, it is possible to deduct that POF sensors were capable of detecting both initial hairline flexural cracks and final failure in plain concrete specimens and steel reinforced concrete beams. The use of a POF sensor to monitor damage in civil engineering structures offers clear advantages over fragile glass-based optical fiber sensors. Their glass-based counterparts tend to fracture in the presence of severe stress concentrations such as cracks losing their sensing function almost immediately after the onset of initial damage. In addition, glass-based optical fiber sensors are susceptible to chemical attack under alkaline and aqueous environments such as those frequently encountered in concrete structures; POFs do not suffer this limitation, highlighting the potential advantages of using these sensors in civil engineering applications.

Inaudi D. *et al.* (2006) produced a strain sensing tape to allow such a good bonding. For producing such a tape, glass fiber reinforced thermoplastic with PPS matrix was used. Polyimide-coated optical fibers were used for the bonding between the optical fiber coating and the matrix. The use of such sensing tape (called SMARTape) was twofold: it could be used externally, attached to the structure, or embedded between the composite laminates, having also a structural role.

Falah M. W. *et al.* (2007) investigated the development of a Fiber Optic Bragg Grating Sensor (FOBGS) for embedding in concrete members to measure strain and monitor cracks. Tests were carried out on a steel plate subjected to flexural stress and reinforced concrete beams subjected to axial tensile stress and temperature change. The FOBGS was employed to track the behaviour of these members under loading conditions. A steel plate of 736.6 x 25.4 x 6.35 mm was tested as a cantilever fixed at one end and free at the other end. The plate was subjected to a vertical concentrated load at the free end with a cantilever span of 376 mm. An FOBGS was installed at the distance of 63.5 mm from the fixed end. The tensile strain was monitored with an incremental load increase from 5 N to 50 N. The temperature during this test was kept constant at 25^{o} C. This test is done to check the performance and the results of the FOBGS before using it in the reinforced concrete specimens. Fig. 2.13 shows the measured strains using the fiber optic sensor. The theoretical strains are plotted in the same figure

for comparison purposes. Fig. 2.13 shows that the experimental tensile strain is almost linear. Comparing the experimental and the theoretical results, it can be seen that the measured strains were within a percentage of 5% higher than the theoretical strains. The maximum difference was noticed at the final load increment.

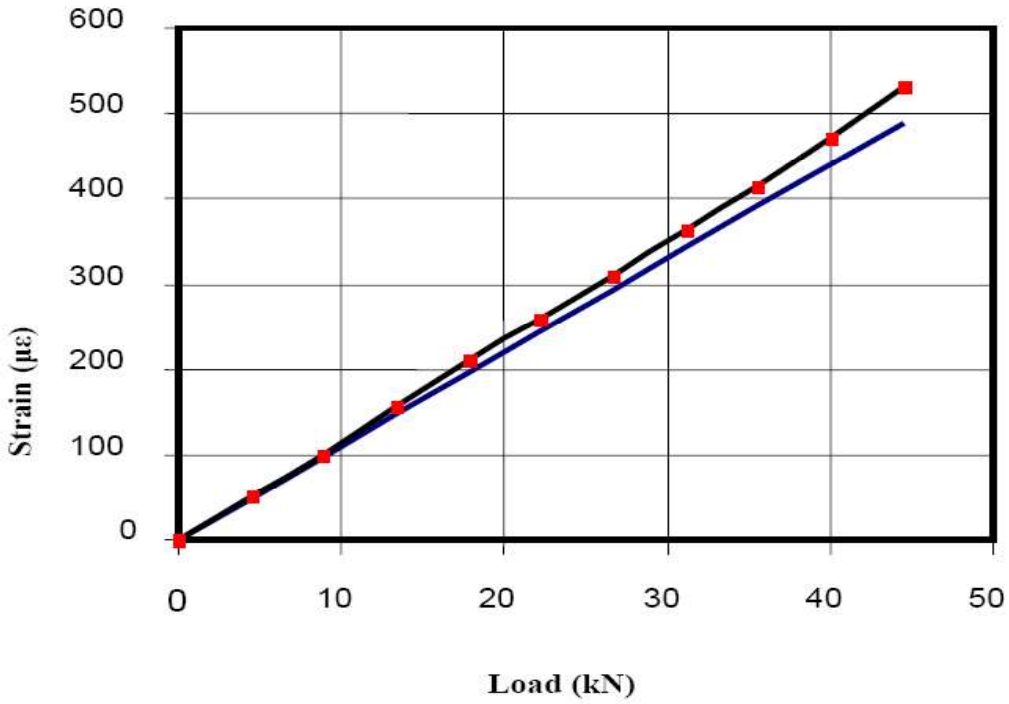

Fig. 2. 13 Tensile Strain in tested steel plate. (Falah M.W. *et al.* (2007)).

The beams with a 160 mm x 160 mm cross-section and 1200 mm length were instrumented by embedded FOBGS to measure strain and monitor concrete cracks. Two specimens, T1 and T2, are subjected to temperature change test, and the remaining two specimens, L1 and L2, are subjected to axial tensile load up to failure. In specimens T1 and L1, the BG sensor is installed at mid-length of one of the main steel bars inside the concrete. In specimens T2 and L2, the BG sensor is attached to a steel plate embedded at the center of the concrete beam. The steel plate is welded to the adjacent stirrups before casting the concrete. The temperature change test is done to examine the temperature sensitivity of the FOBGS measurements. The reinforced concrete specimens T1 and T2 are tested in the climate chamber under a cycled temperature change. During the test, the temperature is increased from the room temperature of 25^{o} C to 45^{o} C in 4 hours,

then decreased to 5° C in 8 hours, and finally increased again up to 25o C in 4 hours. The change in temperature is applied in increments of 5° C per hour. Fig. 2.14 shows the FOBGS recorded strain results for this test. It can be seen from Fig. 2.14, that the relationship between strain and temperature increase is linear. The strain readings are not affected by the low or high temperatures within the experiment range. Therefore, BG sensors can be used for monitoring purposes in the field applications without any measurement interruptions in the normal weather conditions.

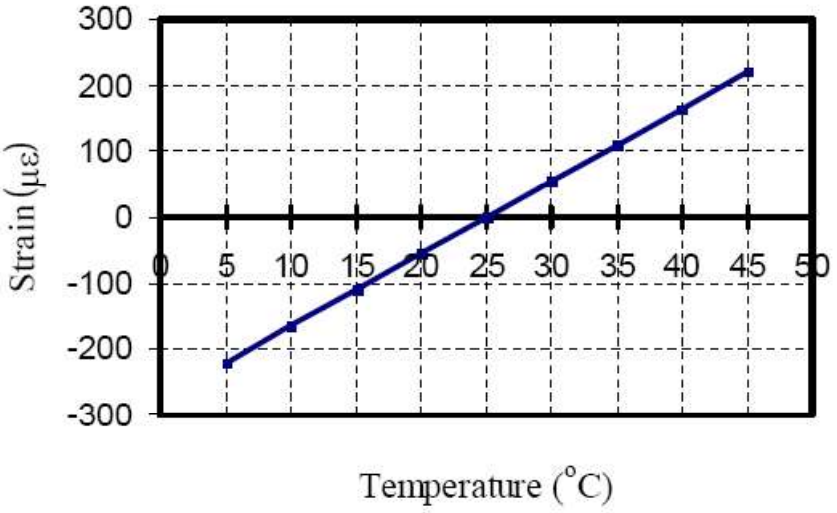

Fig. 2. 14 FOBGS Strain Due to temperature change. (Falah M.W. *et al.* (2007)).

Before applying the tensile load test on specimens L1 and L2, their curing behavior is examined. The concrete beams are fully submerged in water for 28 days. During this period, the FOBGS readings are recorded. The test is done to examine the transmission of the FOBGS signal for long time and in the under-water conditions, and to monitor the behavior of the specimens during the curing period. Fig. 2.15 shows the FOBGS readings for both specimens for the curing duration of 28 days. It can be seen that the voltage readings are increasing in the first 7 days of the test. Here the increase in voltage denotes a decrease in strain. The readings are then fluctuating up and down starting from day 7 until day 28. Finally, the readings remained constant for the rest of the experiment. The results show that the variations in the FOBGS output took place in the first 28 days of the curing time. This is the curing period recommended by the codes of practice in concrete structures. Only minor changes occur in concrete strength after this

period. Specimens L1 and L2 are then prepared for the axial tensile test. The loading system consisted of a hydraulic power supply, a load cell, two carbon fiber reinforced polymer CFRP wires and two shackles. The tensile loads were applied gradually from zero to 90 kN and then back to zero. The FOBGS strain history is recorded and the results show small strain values before concrete cracking. After cracking, the total load is practically carried by the reinforcing steel bars.

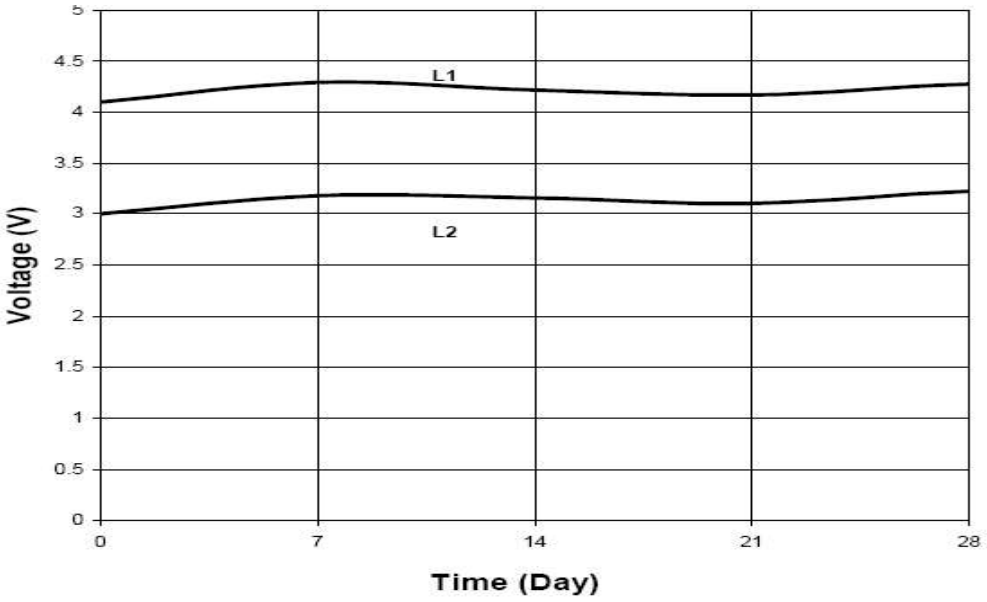

Fig. 2. 15 FBG sensor readings during the curing process. (Falah M.W. *et al.* (2007)).

Specimens are then prepared for the axial tensile test. The tensile loads were applied gradually from zero to 90 kN and then back to zero. Then FOBGS strain history is recorded. The small strain values are observed before concrete cracking. After cracking, the total load is practically carried by the reinforcing steel bars.

Surre F. *et al.* (2012) did comparative study on the fiber bragg grating sensors. Two type of sensors namely; temperature sensors and strain sensors were covered under this study (namely, OSG1, OSG2 are the temperature sensors while OSA, OSB and OSC were strain sensors) . The variation was brought in the installation /mounting process of the sensors. Along with five optical sensors, electrical resistance strain gauges and demountable mechanical strain gauges were also used. RC beam of size 5200mm x300mm x 250mm was casted with 3-16 bars at the bottom and 2-12 bars at the top with a clear cover of 30mm in both

top and bottom. The test program consisted of 3 tests in which, firstly, the specimen was loaded upto 5kN in a step wise manner, and secondly a direct load of 4kn was given to the specimen. Thirdly, beam was loaded in a step wise manner to 20kN and strain vs. time plots were compared for analysis.

For test-1 and test-2 similar observations were made, OSG1 and OSG2 were in good agreement with that from the electrical resistance strain gauge, OSA & OSB appeared to under-read the strain, while the output from OSC suggested the opposite and over-read the strain. While for test -3, OSG2 & OSC were the only ones that remained in good agreement with the electrical resistance strain gage while other sensors, either failed to report any result or under-estimated the results. Key difference in the measurements arise from the fact that OSG family calculated strains only while OSA,B,C family measured only local strains. Thus, for longer runs of health monitoring tests longer gauge devices, mounted securely, gives the best result.

2.4 Effect of GFRP on the behavior of beams

Fiber laminates such as CFRP, GFRP have been a topic of interest for the researchers from a very long time. Laminate's effect on the concrete structure's strengthening/ retrofitting has been used in carrying many researches. FRP's are used in the form of FRP bars as replacement to steel, or as sheets for wrapping and strengthening the structural elements etc.

Ritchie *et al.* (1991) tested sixteen RC beams with minimum steel reinforcement to study the effects of external strengthening using three different types of FRP; glass, carbon, and aramid fibers. The beams were tested in flexure under four-point loading. They developed an analytical model to predict the strength and stiffness of the FRP strengthened beams. The results showed an increase in stiffness from 17% to 99% and an increase in strength of 40% to 97% based on the type, amount, and orientation of FRP that was applied to the beam.Also, the predicted and actual behavior showed good agreement, except that the analytical model predicted a slightly stiffer response than that which was achieved during the tests. They also investigated anchorage methods for the FRP. The first consisted of anchoring the ends of the plate with fiberglass angles. This led to a larger load capacity, but the failure was still located at the ends of the plate. The

second method consisted of wrapping FRP plates around the beam at the ends. This type also raised the load capacity, but was unsuccessful in transferring the failure to the constant moment region. The final method consisted of extending the plates up to the supports. This method was very successful in both increasing the load capacity and shifting the failure to the constant moment region.

Saadatmanesh and Ehsani (1991) experimentally investigated the static strength of RC beams strengthened by gluing GFRP plates to their tension surfaces. Five rectangular beams cross-sections and one T-beam were tested to failure under four-point bending. The measured load versus strain in GFRP plate, steel rebar, extreme compression fiber of concrete, and the load versus deflection for the section at mid-span of the beams were plotted and compared to the predicted values. It was found that the flexural strength of RC beams can be significantly increased by gluing GFRP plates to the tension face. In addition, the epoxy bonded plates improved the cracking behavior of the beams by delaying the formation of visible cracks and reducing crack widths at higher load levels.

An *et al.* (1991) developed a model to predict the stresses and forces of a RC beam with externally applied GFRP. Their study was based on five assumptions: (a) linear strain distribution throughout the beam, (b) small deformations, (c) tensile strength of concrete was ignored, (d) shear deformation was ignored, and (e) perfect bond between concrete and GFRP. Using classical flexural theory and strain compatibility, affects of variables such as material strength, modulus of elasticity, and reinforcement ratios of the steel and GFRP were compared with experimental results of a previous test. The behaviors of the beams were predicted with reasonable accuracy using the model.

Bhutta (1993) studied Moment, stiffness, and deflection models of reinforced concrete beams with applied FRP. Glass, carbon, and kelvar fiber reinforced plastics were utilized. Beams reinforced with kelvar showed the highest increase in moment capacity and stiffness, while the smallest was the beams reinforced with glass. The moment capacity of beams reinforced with carbon fell between these two composites.

The technique of strengthening of RC structures with externally bonded FRP was investigated by **Triantafillou (1998)**. The RC beams are strengthened with externally bonded FRP sheets both in flexure as well as shear zone. Effect on the stress distribution, initial cracks, crack propagation and ultimate strength was studied. For the strengthened beams, ultimate strength significantly increased in comparison to normal beam. The beams strengthened in both flexure and shear had a slight advantage in the ultimate strength, in comparison with beams that were strengthened in flexure only.

In another study by **Li *et al.* (2001)**, the authors strengthened RC beams with externally bonded CFRP sheets. They experimented with beams strengthened differently. One of the beams was strengthened in flexure only, while others were strengthened in both, flexure and shear. They found that for strengthened beams the ultimate strength increased in comparison with normal beam. The increase of strength was found to be higher in the beams that were strengthened both in flexure and shear.

Tavares D.H. *et al.* (2008), studied the behavior of reinforced beams reinforced with GFRP bars. Six beams in which one was control reinforced with deformed steel bars and five reinforced with longitudinal GFRP bars were casted. During testing steel –reinforced concrete beam developed less cracks than that developed in the GFRP-reinforced beams. The results showed that the relatively low modulus of elasticity and high GFRP rupture strain are the main variables that influence the flexural behavior of the GFRP reinforced concrete.

Meda A.*et al.* (2014), studied the flexural behavior of RC beams in which they also aimed to show the influence of fiber reinforcement. Along with fiber reinforcements hooked steel fibers were also used in two different percentages. Later on it was concluded that FRC can modify the collapse mode of beams, bearing capacity of beams can be enhanced but depends on the ratio between FRC toughness and the reinforcement ratio. Overall ductility is strongly influenced by fibres, either in positive or negative terms, depending once again on the FRC toughness and reinforcement ratio. Fibers significantly enhance the behavior at service conditions by increasing the stiffness in the cracked-stage

and, therefore, by limiting the crack openings and deformations. A clear relation between beam behavior at service load and fiber content was also observed.

Thus, it can be concluded that though a lot of research has been done in this area, a lot of scope still remains.

2.5 Vibration monitoring of beams

Salawu (1997) studied the use of natural frequency as a diagnostic parameter in structural assessment procedures using vibration monitoring. The approach was based on the fact that natural frequencies are sensitive indicators of structural integrity. Thus, an analysis of periodical frequency measurements can be used to monitor structural condition. Since frequency measurements can be acquired, the approach could provide an inexpensive structural assessment technique. Factors which could limit successful application of vibration monitoring to damage detection and structural assessment were also discussed, along with the relationships between frequency changes and structural damaged.

A numerical simulated study of damage detection in structures was carried out by **Maia *et al.* (2003).** They also casted a simple beam in order to compare 'mode shape change' based damage detection methods.A generalization of such methods to the whole frequency ranges of measurement was proposed, i.e. methods based on mode shape changes be based on operational mode shapes. The objective of study was to ascertain the possibility of using various damage detection methods without the need for modal identification. Also, a new approach of FRF-based method was presented.

Kim J.T. *et al.* (2005) did vibration-based damage monitoring in model plate-girder bridges under uncertain temperature conditions. The feasibility of using model for damage detection, however, is limited when the changes go undisclosed due to uncertain temperature conditions, particularly for large structures. In this paper, a vibration-based damage monitoring scheme gives warning of the occurrence, the location, and the severity of damage under temperature-induced uncertainty conditions is proposed. Firstly, experiments on a model plate-girder bridge, for which a set of modal parameters were measured under uncertain temperature conditions, are described. Secondly, a damage

warning model is selected to statistically identify the occurrence of damage, by recognizing the patterns of damage-driven changes in natural frequencies of the test structure, and by distinguishing temperature-induced off-limits. Thirdly, a frequency-based damage index method based on the concept of modal strain energy is implemented into the test structure to predict the location and the severity of damage. In order to adjust the temperature induced changes in natural frequencies that are used for damage detection, a set of empirical frequency correction formulae are derived from the relationship between temperature and frequency ratio.

Baghiee *et al.* (2009) studied damage and CFRP strengthening of RC beams by vibration monitoring. They focused on the use of mode shapes and their derivatives. The "Modal Assurance Criterion" and "Coordinate Modal Assurance Criterion" factors were used to detect damage. These factors were derived from mode shapes and modal curvatures. They found that the modal assurance criterion was subjected to very small change by damage or strengthening. The coordinate modal assurance criterion factors detect the changes in beam stiffness at degree of freedom.

An attempt to analyze the natural vibration of monolithic beams with longitudinal cracks for developing a method for its detection was made by **Thalapil J *et al.* (2014).** Analytical method has been developed to address both forward problem of determination of natural frequencies knowing the beam and crack geometry details as well as inverse problem of detection of crack with the knowledge of changes in the beam natural frequencies. Both long (Euler–Bernoulli) and short (Timoshenko) beams have been examined numerically. For modeling a crack located at the free end of a cantilever, the beam is divided into three segments. For an internal crack located away from the free end of the beam, it is split into four segments. In both cases, two of the segments take care of beam portions above and below the crack. The cracked segments are constrained to have the same transverse displacements but different axial deformations. The modeling shows good accuracy for both the forward and inverse problems. The results thus show encouraging possibility of exploitation of the proposed method for crack detection**.**

2.6 Closing Remarks

In this chapter, a small compilation of the previous works done by the various researchers has been presented so that an outline of the work to be done can be sketched up. This chapter carries the information about FBG sensors, flexure behavior of beams, GFRP and vibration monitoring. All these things have not been used together for study of behavior of beams from a long time. So, in this report it is aimed to use these sensors and derive meaningful results.

CHAPTER-3

EXPERIMENTAL PROGRAM

3.1 General

The prime objective of this study was to study the flexural behavior of pre-damaged RCC beams and later on strengthening them with the help of Glass fiber reinforced polymer (GFRP). This chapter carries the detail about the entire experimental program from materials used in casting of beams to strengthening of beams along with the methodologies used for the testing the beams.

The test program for the experimental study comprised of following steps:-

- Determination of properties of the materials to be used in the current study namely cement, sand, coarse aggregates and steel bars as per relevant Indian standard specifications.
- Six RCC beams were casted of size (4100 x 135 x 230 mm) using two different target strengths of concrete, of which three beams were of one target strength and the other three were of second target strength.
- Out of three beams for each grade, one beam was kept as control beam, while other two were pre-damaged upto 50% and 70% of yield load (of each target strength).
- After the beams were pre-damaged by 50% and 70% of yield load GFRP strengthening was applied to the beams to strengthen the beams.
- At every step, i.e., before any damage, after pre damage and after GFRP was applied vibration monitoring of the beams was done.
- All the beams were tested under static loading, to study the flexure behavior of beams.

3.2 Materials

The materials are the key to achieving the desired target strength. In this study two normal strength concrete mixes were used in the casting of RCC beams of size (4100 x 135 x 230 mm). After then the RCC beams were strengthened by GFRP. So, different numbers of constituent materials have been used in the whole studies which are presented as follows:-

3.2.1 Cement

PPC flyash based cement (manufactured by UltraTech Cement Pvt. Ltd.) conforming to IS 1489:1991 from single lot was used for preparing concrete mixes throughout the course of this study. The cement samples were collected and tested according to the guidelines of IS 4031 (Part-11):1988, IS 4031 (Part-5):1988, IS 4031 (Part-6):1988. The physical properties the cement are presented and compared with the requirements of IS 1489:1991 in Table 3.1.

Table 3. 1 Physical properties of cement

S.No.	Characteristics	Obtained Value	IS 1489:1991 (Reaffirmed 2005) Recommended Value	IS codes referred for Test
1.	Specific Gravity	3.06	-	IS 4031 Part 11
2.	Standard Consistency (in %)	34	-	IS 4031 Part 4
3.	Setting Time (min.) Initial Final	 54 205	 30 min., *Min.* 600 min., *Max.*	IS 4031 Part 5
4.	Compressive Strength 3 Days (MPa) 7 Days (MPa) 28 Days (MPa)	 17.060 25.64 37.34	 16 MPa, *Min.* 22 MPa, *Min.* 33 MPa, *Min.*	IS 4031 Part 6
5.	Soundness by Le Chatlier's method (in mm)	2	10 mm, *Max.*	IS 4031 Part 3

3.2.2 Aggregates

Aggregates fill maximum volume of the concrete and are assumed to have a high impact on the properties of concrete. The aggregates should be in proper shape and size, clean hard and well graded. Based on the size of the particle, the aggregates are divided into two groups

- **Fine Aggregate –** The particle size is less than 4.75 mm and,
- **Coarse Aggregate –** The size of the particle is more than 4.75 mm.

3.2.2.1 Fine aggregates

Locally procured sand was used as fine aggregates. The particle size distribution (sieve analysis) and other physical properties of the fine aggregate are presented in Table 3.2 and Table 3.3 respectively. The sand was first sieved through 4.75 mm sieve to remove any particles greater than 4.75 mm and then it was washed to remove the dust. The fine aggregates were tested per Indian Standard Specifications IS : 383-1970.On the basis of particle size distribution, the fine aggregates fall under zone II of IS : 383-1970.

Table 3. 2 Sieve analysis of fine aggregates

I. S. Sieve	Weight retained (gm)	Percentage weight Retained	Cumulative % of weight Retained	Cumulative % of weight Passing	Limit by IS 383 for Zone-II
4.75 mm	13	1.3	1.3	98.7	90 - 100
2.36 mm	10	1	2.3	97.7	75 – 100
1.18 mm	385	38.5	40.8	59.2	55 – 90
600 µm	169	16.9	57.7	42.3	35 – 59
300 µm	267	26.7	84.4	15.6	8 – 30
150 µm	120	12	96.4	3.6	0 – 10
Pan	36	3.6	-	-	
Total	1000	100	282.9		
Fineness Modulus			**2.829**	**Hence, Zone-II**	

Table 3. 3 Physical properties of fine aggregates

Characteristics	Obtained Results	Requirements as per IS 383:1970
Grading	Zone-II	Zone-II
Fineness Modulus	2.829	2.0 to 3.5
Weight of saturated sand A (gm) Weight of pycnometer with sand B (gm) Weight of pycnometer with Water C (gm) Weight of Oven dry aggregate D (gm) **Specific gravity** = (A/ [A-(B-C)]) =	500 1833 1522 560 2.65	 2.6 to 2.7
Weight of saturated sand A' (gm) Weight of Oven dry sand B'(gm) **Water Absorption** = (B'-A')/ (A')	1000 984 1.6%	

3.2.2.2 Coarse aggregates

Crushed stone aggregates (locally available) of 20mm and 10 mm are used throughout the experiment study. The particle size distribution and physical properties of coarse aggregates are given in Table 3.4, Table 3.5 and Table 3.6.

Table 3. 4 Sieve analysis of 10 mm coarse aggregates

I. S. Sieve	Weight retained (gm)	Percentage weight Retained	Cumulative % of weight Retained	Cumulative % of weight Passing	Limit by IS 383
80 mm	0	0	0	100	-
40 mm	0	0	0	100	-
20 mm	0	0	0	100	-
12.5 mm	0	0	0	100	100
10 mm	813	16.26	16.26	83.74	85 to 100
4.75 mm	3643	72.86	89.12	10.88	0 to 20
2.36 mm	289	5.78	94.9	5.1	0 to 5
Pan	255	5.1	-	-	
Total	5000	100	200.28		
Fineness Modulus			$\frac{200.28 + 400}{100}$	**=6.0028**	

Table 3. 5 Sieve analysis of 20mm coarse aggregates

I. S. Sieve	Weight retained (gm)	Percentage weight Retained	Cumulative % of weight Retained	Cumulative % of weight Passing	Limit by IS 383
80 mm	0	0	0	100	-
40 mm	0	0	0	100	100
20 mm	114	2.28	2.28	97.72	85 to 100
10 mm	4567	91.46	93.62	6.38	0 to 20
4.75 mm	301	6.02	99.64	0.36	0 to 5
2.36 mm	12	0.24	99.88	0.12	-
Pan	06	0.12	-	-	
Total	5000	100	295.42		
Fineness Modulus			$\frac{295.42 + 400}{100}$	**=6.9542**	

Table 3.6 Physical properties of coarse aggregates

Characteristics	Obtained Results for 10mm	Obtained Results for 20mm	Requirements per IS 383:1970
Fineness Modulus	6.003	6.954	5.5 to 8.0
Specific gravity	2.68	2.77	2.6 to 2.8
Water Absorption	0.17%	0.37%	-

3.2.3 Water

Water is very important element of concrete mix. The water for both mixing and curing of concrete should be free from unwanted harmful materials. It's generally advised that the water to be used should be free from organic matter, silt, oil, sugar, chloride and acidic material. Thus, potable water is usually used for this purpose. In the present study potable tap water was used during the entire casting and curing period.

3.2.4 Super-plastcizer

Commercially available water-reducing admixture namely 'CONPLAST SP430' based on sulphonated naphthalene polymers confirming with IS 9103:1999 with specific gravity 1.221 and brown color was used in 3 beams to prepare the slurry of required workability. The properties of super-plasticizer are presented in Table 3.7.

Table 3. 7 Properties of super-plasticizer

S.No.	Properties	Values
1.	Physical State	Liquid
2.	Color	Brown
3.	Odour	Slight/ Faint
4.	pH (concentrate)	7-8
5.	Relative Density	1.221
6.	Water Solubility	Soluble

3.2.5 Steel reinforcing bars

Reinforcing bars of 10 mm, 8 mm diameter were used as longitudinal steel. 10mm-ϕ bars were used as tension reinforcement and 8mm-ϕ bars were used as compression steel and shear stirrups. The minimum yield strength supported by the bars is 500N/mm^2 and minimum ultimate strength supported by the bars is 545N/mm^2 with a minimum elongation of 12%.

3.2.6 Fiber reinforced polymer

The FRP composite used in the present study was of bi-directional E- glass fiber in resin. The properties of the dry fiber reinforced polymer as provided by the manufacturers are shown in Table 3.8.

Table 3. 8 Properties of FRP composite

Type of Fiber	Fiber Weight	Fiber Density	Thickness	Tensile Strength	Elongation at Rupture
E-Glass	360 gsm	2.75 g/cm^3	0.324mm	3400 N/mm^2	4.3%

3.2.7 Epoxy resin

The adhesives used for the wrapping of GFRP were of two types namely; primer and saturant. Each of the two solutions again comprised of two solutions: namely, base and curing agent which were mixed in equal ratios. Before the primer solution was applied to concrete surface, the surface was prepared by means grinding so a smooth surface was there for primer application. Primer solution was used for the surface preparation of the concrete (to fill small pores such that no air gaps remain) prior to the wrapping of GFRP and to provide a clean, smooth surface for saturant application.The saturant solution was then applied after the application of the GFRP to the concrete surface. The properties of both the solutions are given in the Table 3.9 and Table 3.10.

Table 3. 9 Properties of Primer

S.No.	Properties	Values
1.	Mix Proportion	Base : Curing Agent = 1:1 By Weight
2.	Form	Liquid
3.	Mixed Density	1.09 kg/L
4.	Pot Life	60 min. ± 15min.
5.	Drying Time	7-9 Hours
6.	Bond Strength	Failure in Concrete

Table 3. 10 Properties of saturant solution

S.No.	Properties	Values
1.	Mix Proportion	Base : Curing Agent = 1:1 By Weight
2.	Form	Liquid
3.	Mixed Density	1.15 kg/L
4.	Pot Life	30 min. ± 15min.
5.	Bond Strength	>2 N/mm^2
6.	Compressive Strength	70 N/mm^2 at 7days

3.3 Design mix proportions of concrete

Two mix design proportions were used and prepared according to method given in IS 10262: 2009 using the properties of materials as discussed above in Table 3.1 to Table 3.7. For checking whether the prepared mix designs give the required target strength or not 6 cube samples of size 150 x 150x 150 mm were casted for each of the mix which were tested at 7 days and 28 days before casting of beams. The details of the mix design are given in Table 3.11

Table 3. 11 Concrete mix proportions

S.No.		Mix – Proportion-1		Mix – Proportion-2	
1.	Target Strength at 28 days (in MPa)	26.60		38.25	
2.	Slump value (in mm)	75-100		75-100	
3.	Cement (in kg/m^3)	380		400	
4.	Water (in kg/m^3)	191.58		182	
5.	Sand (in kg/m^3)	689.795		674.584	
6.	Coarse Aggregate (in kg/m^3)	1176.419		1200.63	
7.	Super Plasticizer	none		0.5% by wt. of cement	
8.	Cube Compressive Strength (in MPa) (at 7 days)	19.9 19.6 20.3	Avg.= 19.93	26.4 28.8 31.4	Avg.= 28.87
9.	Cube Compressive Strength (in MPa) (at 28days)	26.4 25.2 26.6	Avg.= 26.67	42.8 43.0 42.1	Avg.= 42.63

3.4 Designing, Mixing, Casting and Curing of Specimens

The beam specimens used for experimental study are designed using limit state method (IS-456:2000) as doubly reinforced sections. The beam specimens were reinforced with 2-bars of 8mm diameter at compression face and 2 bars of 10mm diameter at tension face with 6 mm stirrups were spaced at 140 mm c/c.

L-section and cross-section of beam specimens are shown in Fig.3.1

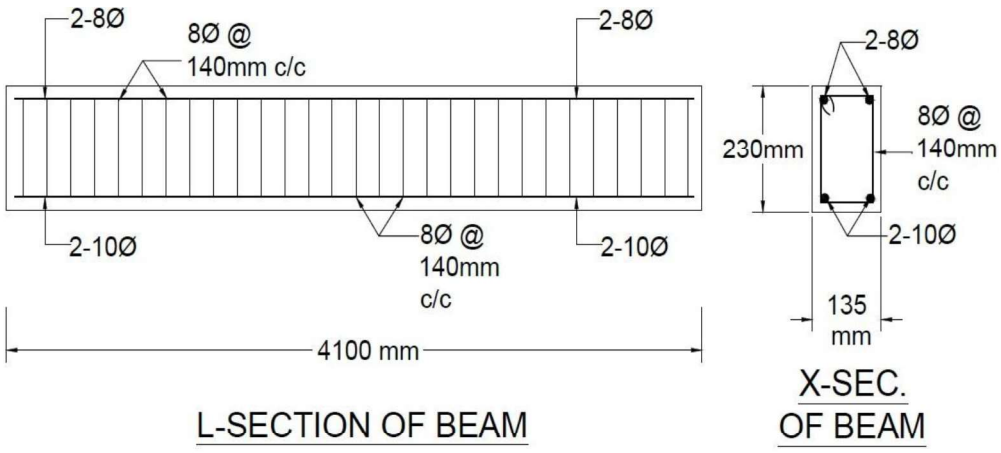

Fig.3. 1 (a) L-section and (b) X-section of the beam specimens used in the study

The measured amount of all the ingredients of the concrete according to the mix proportion viz. cement, sand, coarse aggregate, fine aggregate , water and super-plasticizer (if required according to the mix) were kept ready for each batch of casting. Along with this the molds for the beam specimen and their companion cube specimen were properly bolted and greased before pouring of the concrete mix. Also before pouring the cage of steel was kept inside the mold and to provide clear cover of 20mm, factory made cover blocks were used.

Mixing of the ingredients was done with the help rotary concrete mixer. In the beginning drying mixing was done by adding the sand and cement to the mixer and this mix was mixed until a uniform mix was obtained. Then the coarse aggregates were added to the mix while continuing the dry mixing. Then half amount of measured water was put to the mixer so that the ingredients don not stick to the walls of concrete mixer and a uniform mix can be obtained. After that the remaining water was added to the mix. The total mixing time was about 2-3 minutes and if super-plasticizer was to be used in the mix it was added to the remaining water of the mix. Before the placement of concrete in molds, slump test was performed for each mix; the results are shown in Table 3.12. The mix which was used to fill the slump cone was then used in filling the companion specimen cube molds. For each beam 2 companion specimens were prepared.

Table 3. 12 Results of Slump Test

S.No.	Beam Name	Values of Slump (in mm)
1.	CB21	75
2.	B2-50	72
3.	B2-70	80
4.	CB31	76
5.	B3-50	75
6.	B3-70	78

Fig.3. 2 Slump test of green concrete

The day after the specimens were cast, they were de-molded, marked and covered by wet gunny bags for curing. The curing period lasted for 28 days, 3 times a day after which the specimen were kept in open atmosphere but covered with gunny bags. Fig.3.3 shows the various stages of test specimen during casting and curing.

Before testing the surface of all the specimens were painted with white color to enable monitoring of cracks during the testing. The companion specimens were also tested in ACTM when the beam specimen was tested for 4-point load test.

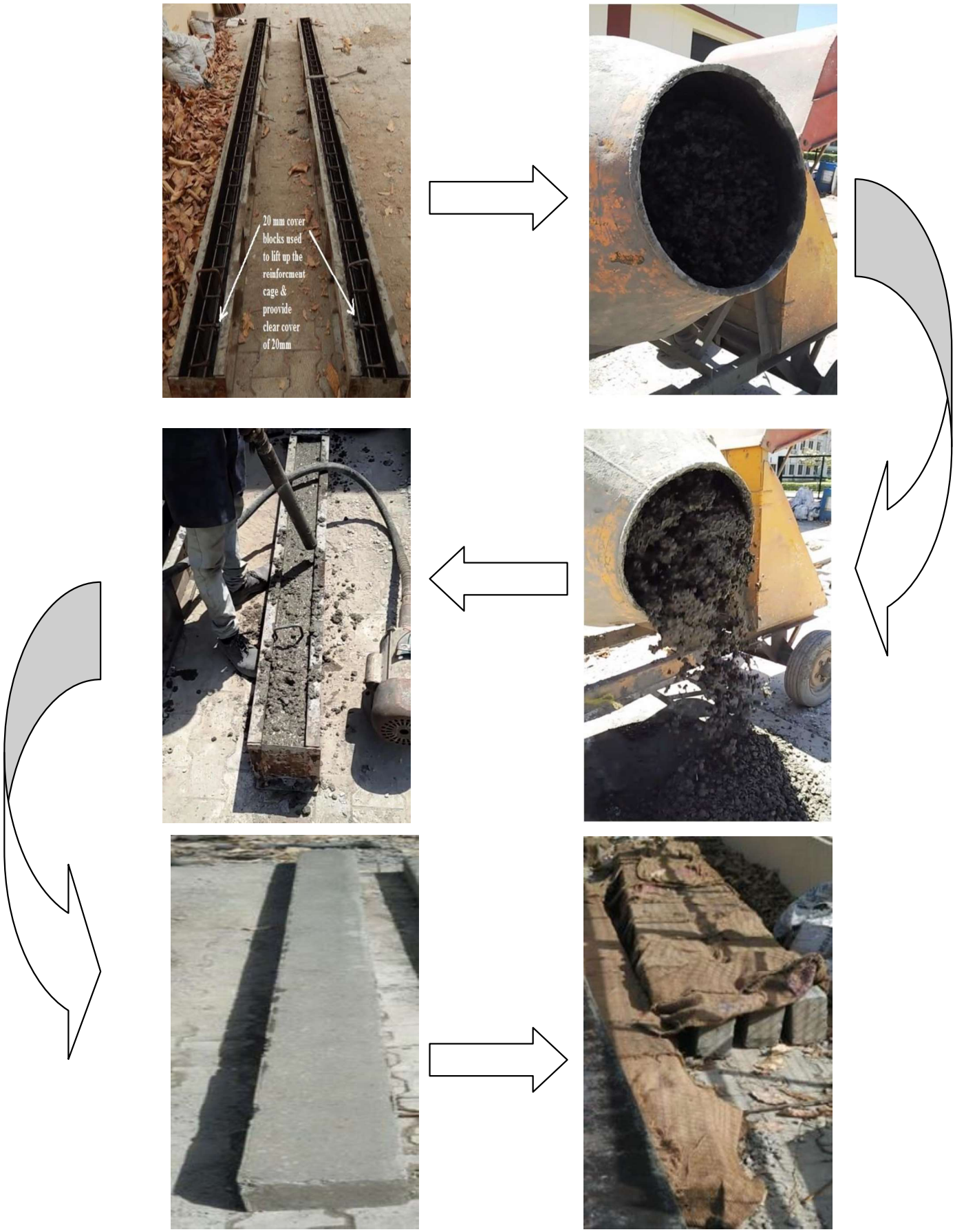

Fig.3. 3 Stages of preparing mold, casting, demolding and curing condition of beam specimen

3.5 Test Setup

Two types of tests were performed on the bema specimens while the companion specimens were tested in the ACTM. The two types of tests are explained as follows:

3.3.1 Vibration Monitoring

This test provides us with the natural frequencies of the material. In this study vibration monitoring was performed to check the health of the beams at different stages i.e., before they incurred any damaged, after the beam specimens were 50% and 70% damaged and when the beams were strengthened by GFRP. Vibration characteristics of all beams were recorded and analyzed by using NVGate 8.3 and Modal 5.2 softwares supplied by OROS solutions.

The FRF (frequency response function) were recorded from the analyzer by striking the hammer above the accelerometer. The position of accelerometers and striking of hammer was pre-decided at L/2 and L/3 distance respectively (indicated by green arrow heads) for accelerometers and at L/2 position (indicated by red arrow head) for hammer striking as shown in Fig.3.4

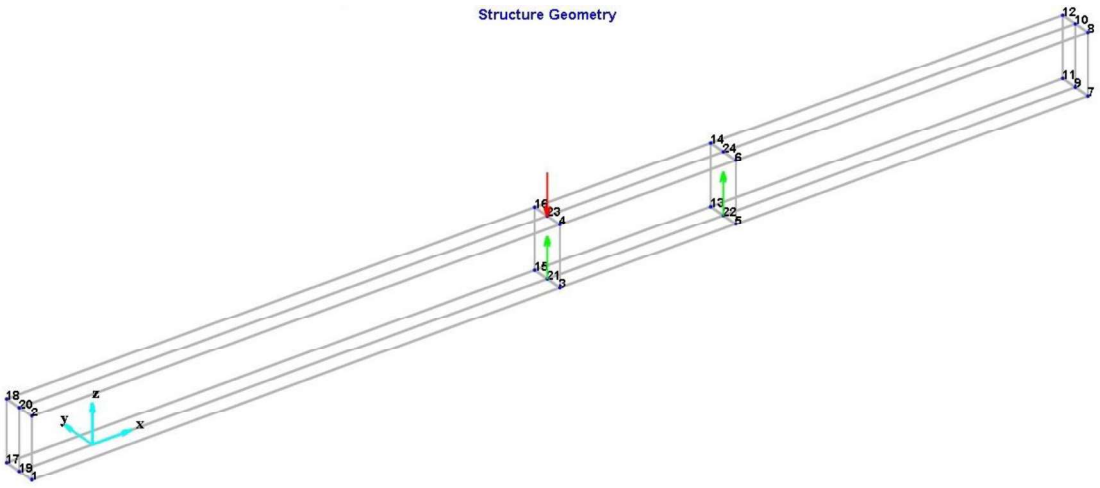

Fig.3. 4 Positon of accelerometers and location hammer strike during a vibration monitoring experiment.

In vibration monitoring experiment two terms are the most important one is triggering and the other one is 'FRF'. Triggering is a technique for capturing an event for which it is not known exactly when it will occur. A trigger can start data acquisition and processing when a user specified voltage level is

detected in an input channel. In the current software FRF is automatically when the trigger is right. But in general it is computed from two signals as it describes the level of one signal relative to another signal. The various components of vibration monitoring setup are shown in Fig.3.5 to Fig 3.6.

Fig.3. 5 Accelerometers used in vibration monitoring

Fig.3. 6 Anlayser that collects all the responses from hammer and accelerometers and provide the FRF

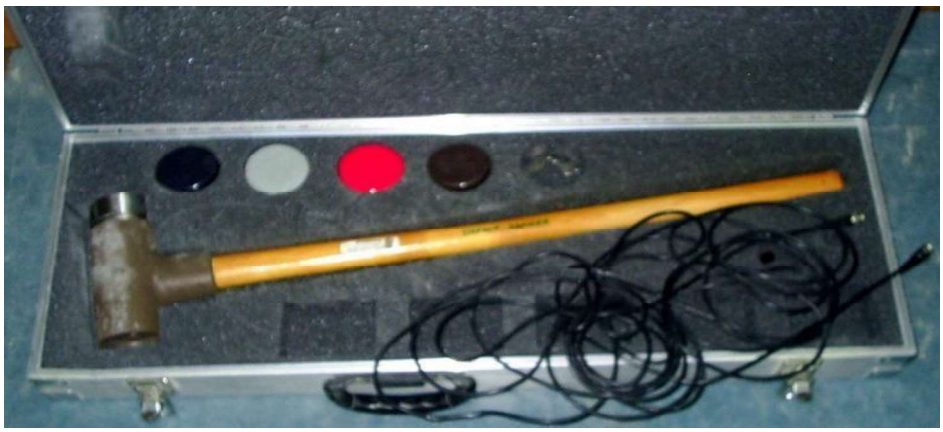

Fig.3. 7 Impact Hammer that is used in vibration monitoring

3.3.2 Four point flexure test

Four point flexure test ensures pure bending (as discussed in introduction part of this report), thus preferred over three point load. The test set up used in this test is shown in Fig.3.8.

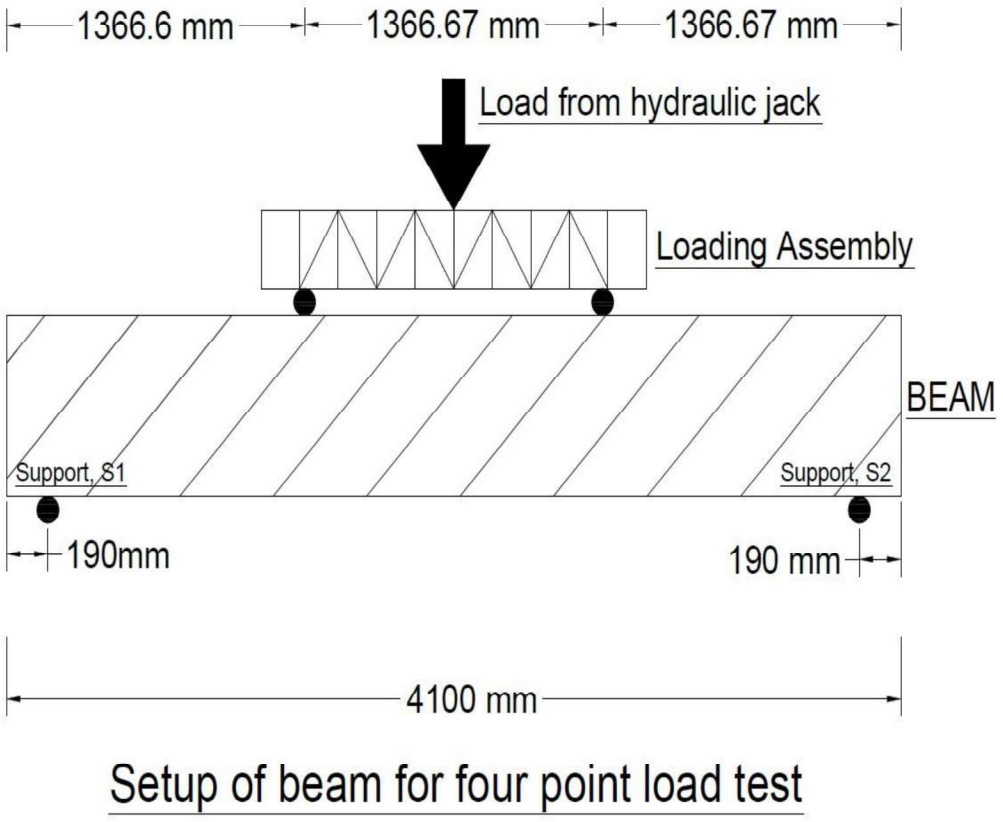

Fig.3. 8 Dimension wise beam setup for four point load test.

In this test along with the optical fiber displacement gage conventional LVDT was also used in measuring the deflection at L/2 distance from the edge of the beam so that to make sure that the displacement recorded by optical displacement gage were correct. Similarly, along with optical strain gage the conventional electrical type strain gage were also put to use, so that there values could be compared. The optical displacement gage, OS5100 and the optical strain sensor, OS3200 have been manufactured by Micron Optics Pvt. Ltd. While the conventional LVDT used was procured from AIMIL Pvt. Ltd. and the conventional strain gage used in this study is PL-90-11 manufactured by Tokyo Sokki Kenkyujo (TML). Fig. 3.9 shows how the optical strain gage and the conventional strain gage were mounted on a concrete beam and Fig. 3.10 shows the whole mounting setup.

Fig.3. 9 (a) PL-90-11 conventional sensor mounted on concrete beam (b) optical strain gage mounted on steel plate which is then pasted on concrete beam using white cement

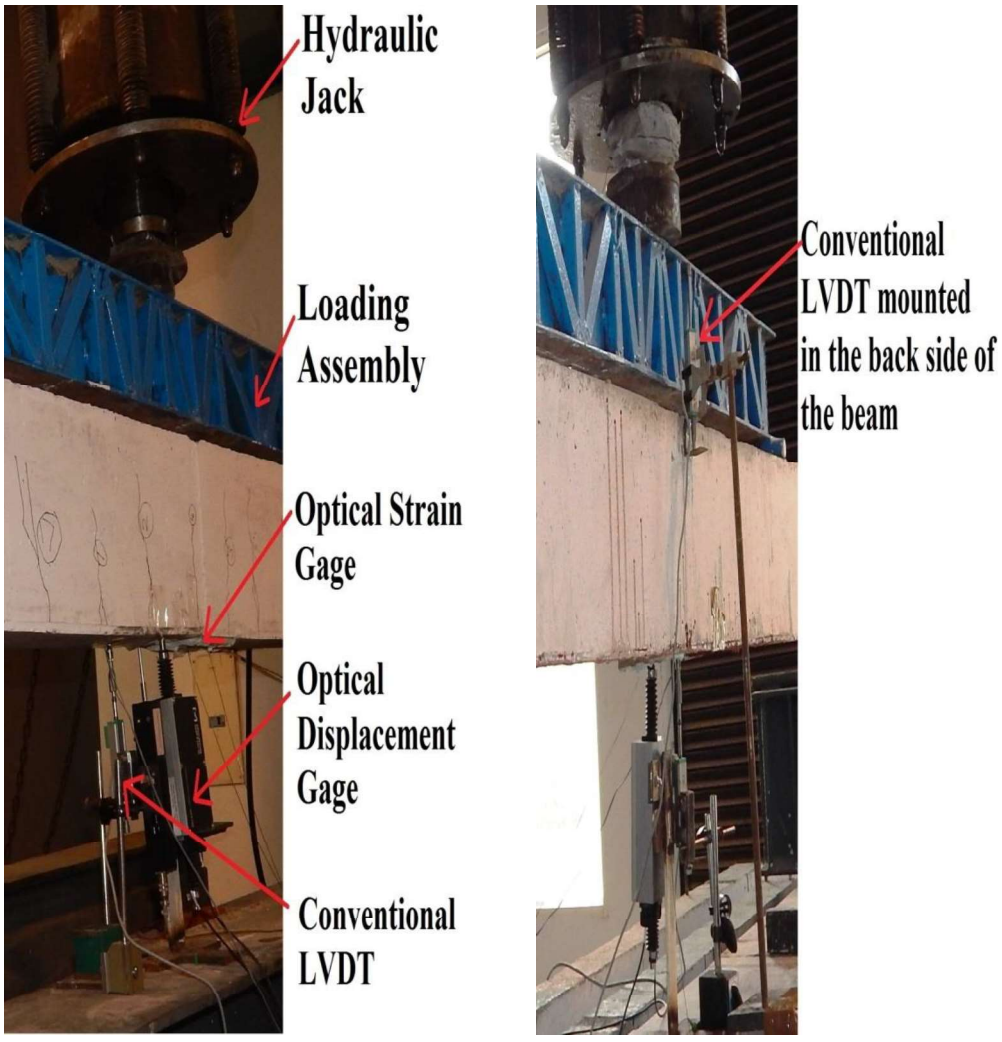

Fig.3. 10 Mounting arrangement of optical strain gage and conventional LVDT on the beam.

CHAPTER-4

RESULTS & DISCUSSIONS

4.1 General

This chapter comprise of all the test results that were obtained while doing vibration monitoring of beams as well as the results obtained when the beam specimen were subjected to load under four point loading. For ease of convenience the following nomenclature was followed for the beams as shown in Table 4.1

Table 4. 1 Nomenclature of beam specimens

S.No.	Assigned Beam Designation	Description
1.	CB21	Control beam Specimen of Mix proportion -1
2.	CB31	Control beam Specimen of Mix proportion -2
3.	B2-50	Beam Specimen of Mix proportion -1 which was pre-damaged by loading it upto 50% of yield load of control beam
4.	B2-70	Beam Specimen of Mix proportion -1 which was pre-damaged by loading it upto 70% of yield load of control beam.
5.	B3-50	Beam Specimen of Mix proportion -2 which was pre-damaged by loading it upto 50% of yield load of control beam.
6.	B3-70	Beam Specimen of Mix proportion -2 which was pre-damaged by loading it upto 70% of yield load of control beam
7.	B2-50S	B2-50 beam specimen after strengthening by GFRP.
8.	B2-70S	B2-70 beam specimen after strengthening by GFRP.
9.	B3-50S	B3-50 beam specimen after strengthening by GFRP.
10.	B3-70S	B3-50 beam specimen after strengthening by GFRP.

4.2 Test Observations

For CB21, the crack pattern is shown in Fig. 4.1, the conventional strain sensor was pasted with adhesive while the optical sensor was pasted on an aluminum plate by epoxy and that plate was pasted to specimen via thin layer of commonly available white cement. The first crack appeared at 10.5 kN near L/3 position. The ultimate load for this beam was 34.470 kN. All the setup was same for beam CB31 and the first crack was observed at around 11.40 kN near middle of the L/2 & L/3 position of the beam. The crack patterns for this beam are shown in Fig.4.2. Beam failed at load of 33.411 kN

For Beam B2-50 and B3-50, the pre-damaging load was equal to 15kN each. The first cracks appeared at around 10.80 kN and at 11.70 kN respectively. Minute cracks which were almost 15-25% of the depth of the beam were generated in both the beams. The crack patterns are shown in Fig.4.3 and Fig, 4.4 respectively. Similarly for beams B2-70 and B3-70, the load was kept upto 21 kN while the cracks started appearing at around 11.10 kN for B2-70 and 11.40 kN for B2-70 and B3-70respectively as can be seen in Fig. 4.5 and Fig.4.6.

After that, strengthening of beams was done by firstly grinding the bottom face of the beam, then the face was cleaned up by using compressed air. After 24 hours of primer application beams were applied with a coat of saturant, on which the GFRP was placed with the help of rollers. And again a single coat of saturant was applied using rollers so that there were no air gaps. After the process of strengthening the beams were ready when the saturant dried. A curing period of 7 days was kept in this case and then the strengthened beams were tested.

After that the beams B2-50S, B3-50S, B2-70S and B3-70S were tested under four point loading. No new cracks formation was observed. Only the previous cracks propagated and widened. The failure of these beams was considered when the GFRP sheet had a brittle failure. The ultimate load for these beams was 35.769 kN, 35.817 kN, 35.23 kN and 35.40 kN respectively, (Fig.4.7 –Fig.4.10). Also, one more thing to be noted was that the optical sensor plate tends to fell down when there was crack propagation at the locations where optical sensor was mounted because the contact between the FRP and concrete got loosened and the plate fell down because of its weight.

Fig.4. 1 Crack patterns of beam CB2-1 when total failure of specimen occurred.

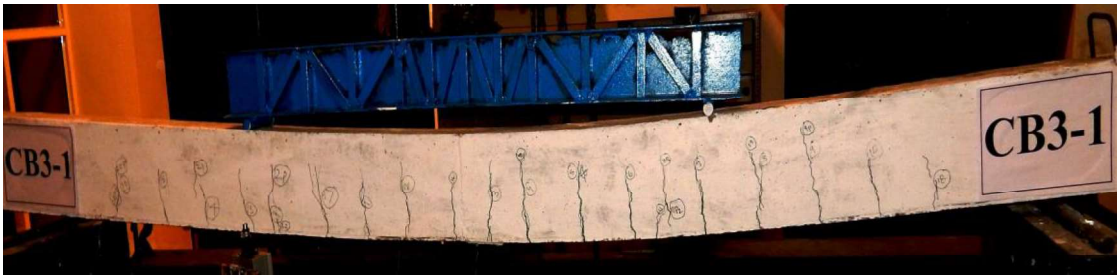

Fig.4. 2 Crack patterns of beam CB3-1 when total failure of specimen occurred.

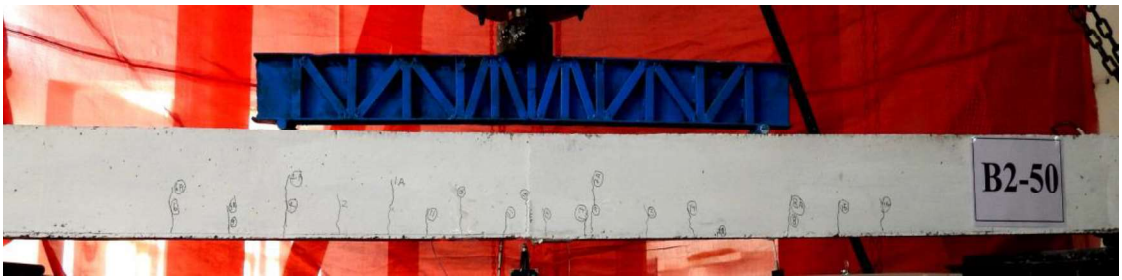

Fig.4. 3 Crack patterns of beam B2-50 when specimen was loaded upto 5kN.

Fig.4. 4 Crack patterns of beam B3-50 when specimen was loaded upto 5kN.

Fig.4. 5 Crack patterns of beam B2-70 when specimen was loaded upto 7KN.

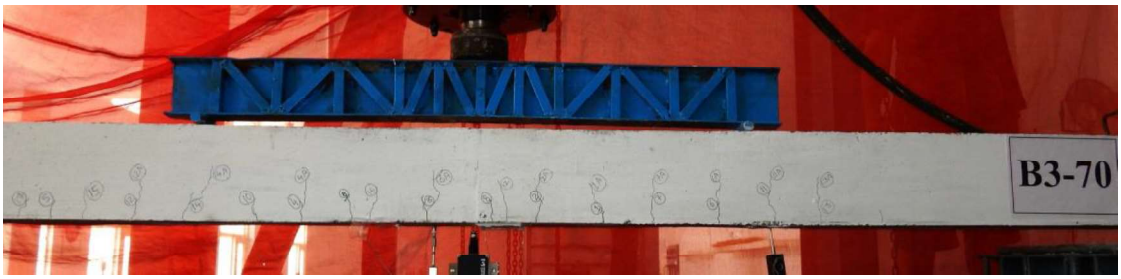

Fig.4. 6 Crack patterns of beam B2-70 when specimen was loaded upto 7KN.

Fig.4. 7 Crack patterns of beam B2-50S when total failure of specimen occurred.

Fig.4. 8 Crack patterns of beam B3-50S when total failure of specimen occurred.

Fig.4. 9 Crack patterns of beam B2-70S when total failure of specimen occurred.

Fig.4. 10 Crack patterns of beam B3-70S when total failure of specimen occurred.

The companion specimens which were casted along with the beams were also tested on following results was obtained:-

Table 4. 2 Test results of companion specimens when beam specimens were tested

S.No.	Companion Specimen of Beam Designation	Strength of Companion Specimen (MPa)	Weight of Companion Specimen (Kg)	Density (Kg/m^3)	Average Compressive Strength of Companion Specimen (MPa)
1.	CB21	39.2	8.209	2432.30	39.4
		39.6	8.759	2595.26	
2.	CB31	51.1	8.343	2472.00	51.55
		52.0	8.324	2466.37	
3.	B2-50	42.2	8.133	2409.78	41.9
		41.6	8.056	2386.96	
4.	B3-50	51.0	8.383	2483.85	51.6
		52.2	8.380	2482.96	
5.	B2-70	40.4	8.058	2387.56	40.8
		41.2	8.254	2445.63	
6.	B3-70	49.8	8.238	2440.89	49.1
		48.4	8.284	2454.89	

4.3 Vibration Monitoring Test

The vibration monitoring test was carried out according to the procedure discussed in section 3.3.1 of this report. FD data and TD data were saved and frequency response function's magnitude values were taken from them (as shown in APPENDIX-A) of this report and the following results were obtained and damage index was calculated by the formula suggested by **Kanwar S. *et al.* (2016):**

$$\text{Damage Index} = \frac{FI_i - FD_i}{FI_i}$$

Where,

FI_i = amplitude of the FRF of the undamaged beam specimen.

FD_i = amplitude of the FRF of the damaged beam specimen.

Table 4. 3 Summary of results for different beam samples as recorded by OROS

S.No.	Beam Designation	First Mode Frequency (in Hz)	FRF Magnitude (in ms^{-2}/N)	Damage Index
Before Application of any Load				
1.	B2-50	20.00	1.340×10^{-1}	0
2.	B2-70	20.00	1.877×10^{-1}	0
3.	B3-50	24.00	1.705×10^{-1}	0
4.	B3-70	23.00	1.989×10^{-1}	0
After providing 50% & 70% damage accordingly				
5.	B2-50	15.00	7.462×10^{-2}	0.4431
6.	B2-70	17.00	6.126×10^{-2}	0.6736
7.	B3-50	15.00	5.954×10^{-2}	0.6508
8..	B3-70	17.00	6.575×10^{-2}	0.6694
After Strengthening with GFRP				
9.	B2-50S	16.00	7.551×10^{-2}	0.4365
10.	B2-70S	18.00	7.092×10^{-2}	0.6222
11.	B3-50S	16.00	7.631×10^{-2}	0.5524
12.	B3-70S	18.00	6.681×10^{-2}	0.6641

The inferences that can be made from the values obtained in table are that every beam has its own natural frequency and similar mix proportion doesn't guarantees the similar natural frequency or similar frequency response function. Damage index of the beams increased as the damaged increased, this can be noticed by observing the damage index for B2-50 and B2-70 beams, for B3-50 and B3-70 similar thing happened. But, damage index got reduced when the beams were strengthened by GFRP. For B2-50, B3-50, B2-70, B3-70, the reduction was around of 1.5%, 15.11%, 7.64%and 0.80 % respectively. So, GFRP strengthening had a positive effect. Strengthening didn't alter the natural frequency of the beams very much but the Frequency response function increased significantly for beams B2-70S and B3-50S, while for other two the increase was minimal.

4.4 Four Point Flexure Test on Beams

Under the flexure test on beams the study of behavior of beams is done by observing the change in two parameters, namely, deflection and strain with respect to the increasing load. The working theory behind the test was discussed in the chapter-1 of this report while test procedure was discussed in section 3.3.2 under chapter-3. In addition to the test procedure discussed earlier it's important to know how these strains and deflections are being calculated with the help of these sensors.

For FBG sensors the change in wavelength is the trigger for calculating the deflection and strains. The rate of data acquisition was 1 kHz that means in a second's time interval 1000 observations were made on account of strain and deflection separately. Deflection was calculated by the interrogator by the formula:-

Displacement, D (in mm) = $m (\lambda_2 - \lambda_1) + b$

Where,

m= gage factor having value of 5.6219mm/mm for E00145, OS5100 optical displacement gage.

λ_2 & λ_1 are the interrogated wavelengths (in nm) obtained from FBG1 and FBG2 respectively.

b = offset = -16.64 mm/mm for E00145, OS5100 optical displacement gage.

Similarly, strain was calculated by the interrogator by the formula:-

Strain, ε (in μm/m) = $\left(\frac{\Delta\lambda}{\lambda_o}\right)$ 1x 10^6 / F_G - ε_{TO}

& Thermally induced apparent strain, ε_{TO} (in μm/m) = $\Delta T\ [C_1/F_G + CTE_S - C_2]$

Where,

F_G = Gage factor =0.796

C_1 = Gage Constant 1 = 6.156 μm/m - ^oC

C_2 = Gage Constant 2 = 0.70 μm/m - ^oC

ΔT = measured temperature change

CTE_s =CTE of test specimen = generally, user defined (in μm/m - ^oC)

$\Delta\lambda$ = wavelength shift, which is interrogated (in nm).

λ_o = nominal wavelength = 1512 nm in this case.

Here, while calculating strains temperature strains were ignored and the formula used to calculate the strain concrete beam was:-

Strain, ε (in μm/m) = $\left(\frac{\Delta\lambda}{\lambda_o}\right)$ 1x 10^6 / F_G, where all symbols have their usual meaning as discussed above.

While for the conventional LVDT (supplied by AIMIL) and strain gage (supplied by TML) work on the change in voltage. LVDT's calculate the deflection by the formula

Deflection (in mm) = -0.016599 + 5.001507x

Where,

x = the output voltage sent by LVDT to the UEI logger.

And strain was calculated by the formula,

$$\text{Strain (in } \mu\text{m/m)} = \frac{4}{\text{G x N}} \text{ X } \frac{x}{\text{Excitation Voltage}}$$

Where,

G= gage factor = 2.15

N= Number of gages being used.

x = the output voltage sent by strain gage to the UEI logger.

Excitation Voltage= 7.5 V

Using these formulas values were calculated by the interrogators and after that the Load vs. Deflection and Load vs. Strain graphs were obtained as results.

4.3.1 Displacement gage results

Load vs. Deflection curves were made based on the values obtained by optical displacement gage and conventional LVDT's. Upon observing both the values obtained from optical & conventional gages were in complete agreement of each other. Thus, here only the graphs presented are based on the deflections obtained by optical displacement gage OS5100.

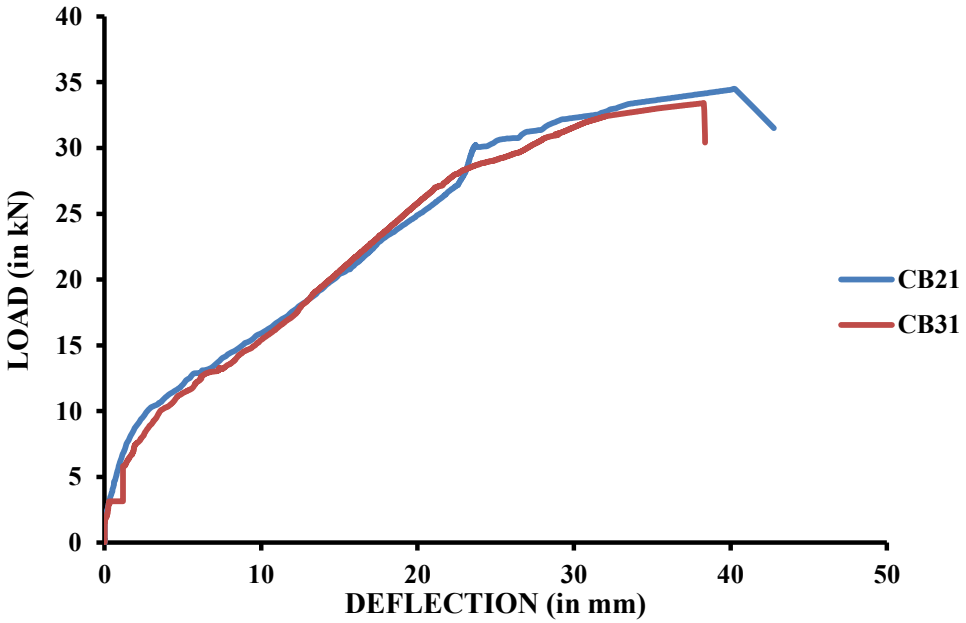

Fig.4. 11 Load vs. Deflection curve for control beams of different mix-proportion

From Fig. 4.11, it can be observed that the behavior of both the beams is same with respect to the deflection, and even the ultimate loads are almost same i.e.

34.47 kN for CB21 and 33.411kN for CB31 for the maximum deflections of 40.3mm and 38.3044 mm respectively. The yield load can be taken up as equal to 30kN for both the control beams (29.23 kN for CB21 and 28.30 kN for CB31) with a yield deflection of 23.360 mm for CB21 and 22.91mm for CB31 respectively. After the testing of these control beams the remaining two beams of each mix-proportion were pre-damaged by 50% and 70% of the yield load of the control beams i.e. applying load of 15kN and 21kN on the remaining two beams of each mix proportion.

From the Fig.4.12, it can be inferred that by strengthening of the beams with GFRP the ultimate load, P_u does not increases for 'B2-50S' (35.769 kN) and 'B2-70S' (35.229 kN) as compared to the ultimate load of 34.47 kN for CB21. Here, by strengthening of beams the stiffness has increased for 'B2-50S' and 'B2-70S' as the beams started deflection at later loads i.e. 16.11 kN and 11.91 kN respectively as compared to the control beam CB21 which started deflecting at 0.45kN. Also, in each curve there is a part when the Load is directly proportional to the deflection, for B2-50S it's from 16.11kN to 34.17kN, for B2-70S it's from 21.18kN to 31.14kN and for CB21 it's from 9.69kN to 29.97kN. Increase in stiffness can also be identified by comparing the behavior of B2-50 with B2-50S and of B2-70 with B2-70S. When the beams have reached upto their yield point, as the deflection increased the rate of change of load decreased. Hence, 19.09 kN, 19.40 kN and 29.23 kN can be are the yield load, P_y for the beams namely B2-50S, B2-70S and CB21 (found by linearization of curves method).

Similarly, for mix-proportion-2 load vs. deflection curves shown in Fig.4.13 were made based on the values of optical displacement gage and load applied. Here also, by strengthening of the beams with GFRP the ultimate load, P_u is not increased as for 'B3-50S' (35.817 kN) and 'B3-70S' (35.400 kN) in comparison to the ultimate load of 33.39 kN for CB31 and by strengthening of beams the stiffness has increased for 'B3-50S' and 'B3-70S' as the beams started deflection at later loads i.e. 22.14 kN and 17.61 kN respectively as compared to the control beam CB31 which started deflecting at 1.44 kN. Increase in stiffness is also evident by comparing the behavior of B3-50 with

B3-50S and of B3-70 with B3-70S. The further summary of load and deflection parameters is shown in table 4.3

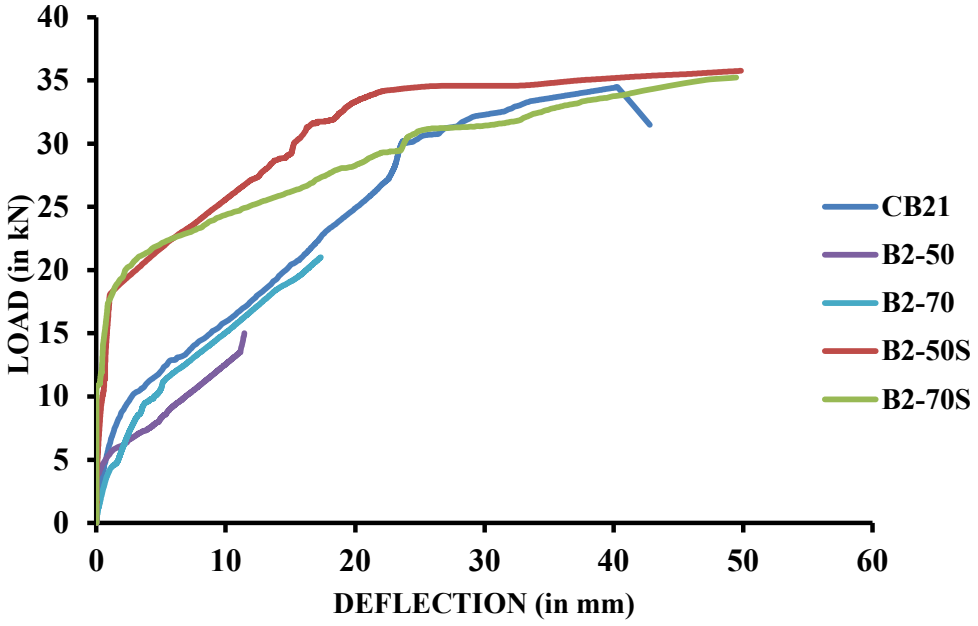

Fig.4. 12 Load vs. Deflection curve for beams of mix-proportion -1

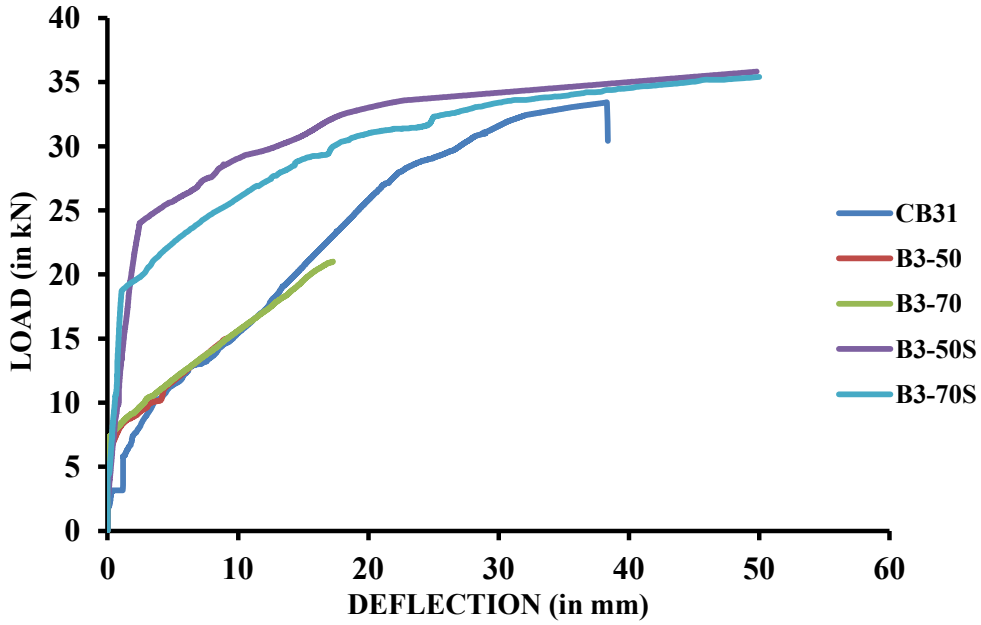

Fig.4. 13 Load vs. Deflection curve for beam specimens of mix-proportion -2

Table 4. 4 Various parameters calculated from load deflection curves of various beam specimens.

Beam Desig.	Load (kN)		Deflection		Deflection Ductility Factor Δ_u / Δ_y	Energy		Energy Ductility Factor $\mu = E_u/E_y$	Energy Dissipation (kN-mm)	Initial Stiffness P_y / Δ_y (kN/mm)	Secant Stiffness P_u / Δ_u (kN/mm	Failure Mode
	Yield Load, P_y (kN)	Ultimate Load, P_u (kN)	Δ_y (mm)	Δ_u (mm)		E_y (kN.mm)	E_u (kN.mm)					
CB21	29.23	34.47	23.36	40.30	1.73	446.36	650.58	1.46	650.58	1.25	0.86	Flexure
B2-50S	19.09	35.77	2.02	49.83	24.63	13.70	357.46	26.09	357.46	9.43	0.72	Flexure
B2-70S	19.40	35.23	1.99	49.49	24.90	9.91	466.97	47.14	466.97	9.76	0.71	Flexure
CB31	28.30	33.39	22.91	38.30	1.67	389.69	611.94	1.57	611.94	1.24	0.87	Flexure
B3-50S	24.52	35.82	3.16	49.81	15.75	38.30	314.25	8.20	314.25	7.75	0.72	Flexure
B3-70S	19.45	35.40	1.98	50.00	25.27	15.23	390.61	25.65	390.61	9.83	0.71	Flexure

From the Table 4.4, it can be observed that both deflection and energy ductility factor for the beams increased with the application of GFRP. The energy dissipation trend for the mix-proportion varied similarly, it was less for the predamaged beams as compared to control beams and for 50% predamaged beams it was less than the 70% damaged beams. Also, the initial stiffness increased for the beams strengthened by GFRP. The stiffness of 70% damaged beams was more than the 50% damaged beams because it may have been possible that the primer-saturant epoxy may have entered the cracks and have come into play. But the secant stiffness results were different where controls beams were having more stiffness than the GFRP strengthened beams.

4.3.2 Strain sensor results

The results obtained from the data sent by the optical strain data and conventional strain gage are used to generate strain vs. time plots and calculate stresses as well tress values were calculated using the formula,

Stress, σ (in N/mm^2) = $\frac{My}{I}$

Where,

M= Bending Moment (in N-mm)

$= \frac{P\ (S_o - S_i)}{4}$

y = Distance to the neutral axis (mm) = D/2

I= Second moment of area (mm4) = BD^3/12

P= Load applied, (in kN).

S_o= c/c distance between the supports, (in mm).

S_i= c/c distance between the supports of loading assembly, (in mm)

B= Breadth of beam specimen, (in mm).

D= Depth of beam specimen, (in mm).

Fig.4.14 and Fig.4.15 shows the variation of strain with time for beam CB21 and beam CB31. Both the sensors are in almost complete synchronization with conventional strain gage. It is to be noted that the strain values of conventional strain gage are higher than that of the conventional strain sensors. Also, for CB21 the conventional sensor values become static when the load of 30.15kN was reached.

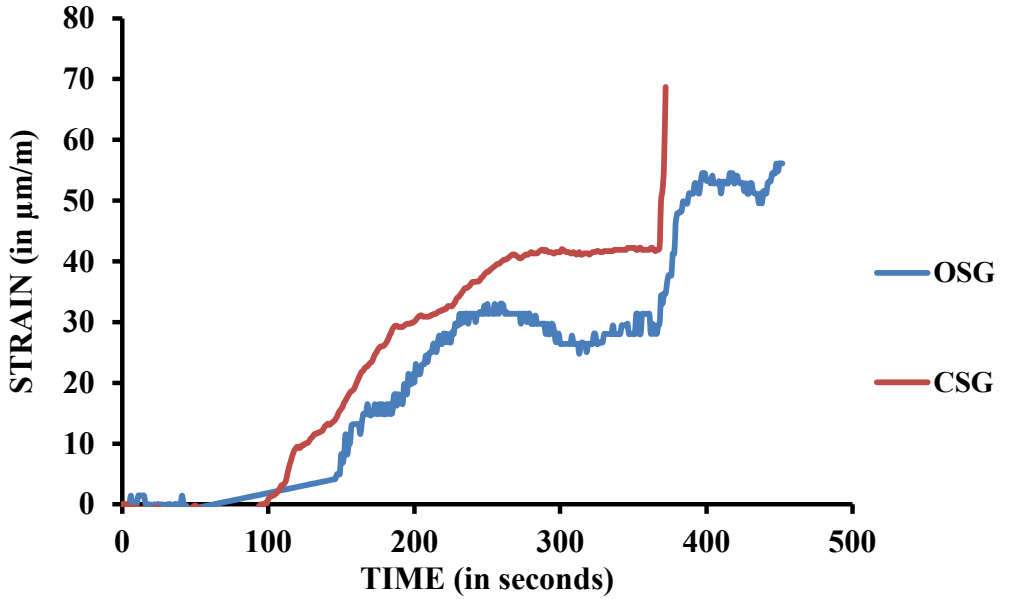

Fig.4. 14 Strain vs. Time curve for beam CB21

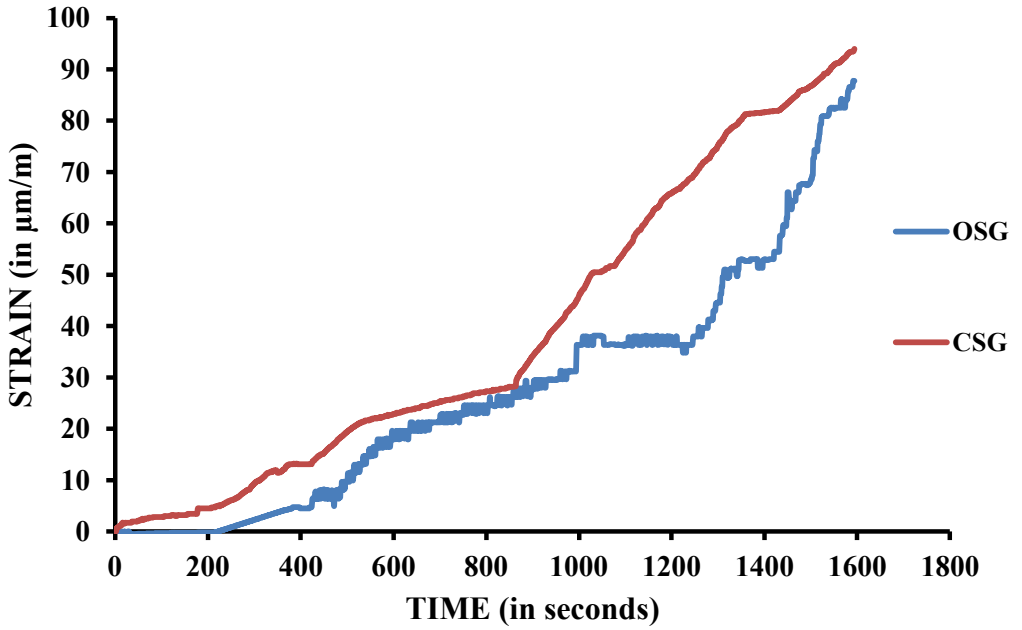

Fig.4. 15 Strain vs. Time curve for beam CB31

From Fig. 4.15, the strain values are in complete agreement of each other and both the sensors worked fine. The maximum strains recorded for beam CB21 are 61.331 microstrains by optical strain gage at 456 seconds and 68.70 microstrains by conventional strain gage at 372 seconds. For CB31 these are 87.75 micro-strains and 94.00 micro-strains respectively.

In terms of stress values, it is observed that the stress taken up by CB21 and CB31 is equal to 15.1254N/mm^2 for CSG (conventional strain gage) and 15.703 N/mm^2 for OSG (optical strain gage), derived by the load of 30.6 kN for CSG and 31.5 kN for OSG respectively at the strains of 61.331 microstrains and 68.70 microstrains for conventional strain gage respectively.

Further, Fig.4.16 to Fig.4.19 shows the strain vs. time plots for the strengthened beams, B2-50S, B3-50S,B2-70S and B3-50S respectively. Two things can be observed from each plot (Fig. 4.17,4.18,4.19) except for B2-50S (Fig. 4.16) the optical strain gages in each plot is showing that the optical strain values are showing the higher side of values as compared to conventional sensors and the values from optical sensor stopped coming very early as compared to other conventional strain sensors. This may be due to the fact that the optical strain sensors fell down as the crack propagation started at their respective locations. For B2-50S maximum recorded strains are 42.88 microstrains and 47.69 microstrains , for B3-50S they are 72.096 and 86.68, for B2-70S they are 64.19 microstrains and 61.3218 microstrains, for B3-70S they are 90.59 microstrains and 77.03 microstrains as sent by optical sensor and the conventional strain sensors respectively.

Also, the calculated stress corresponding to these strains shows that stress corresponding to B2-50S OSG is equal to 15.5258N/mm^2 (31.41 kN) at 61.331 microstrains and 15.6889N/mm^2 (31.74 kN) for CSG at 68.70 microstrains. Similarly, for B2-70S its 12.3672N/mm^2 (25.02 kN) for OSG and 17.4140N/mm^2 (35.23kN) for CSG, for B3-50S it comes out to be 11.8631 N/mm^2 (24.0 kN) for OSG and 16.542 N/mm^2 (33.465 kN) for CSG and for B3-70S its 10.365 N/mm^2 (20.970 kN) for OSG and 17.498 N/mm^2 (35.400kN) for CSG. Thus, on comparing these values with the results obtained from Load vs. deflection curves , it can be concluded that except a few strain gages, none of the strain gages were

able to send strain data up till the end of the test. Either they were delaminated from the surface of the GFRP strengthened concrete beam or malfunctioned by giving unexpected higher amount of strains.

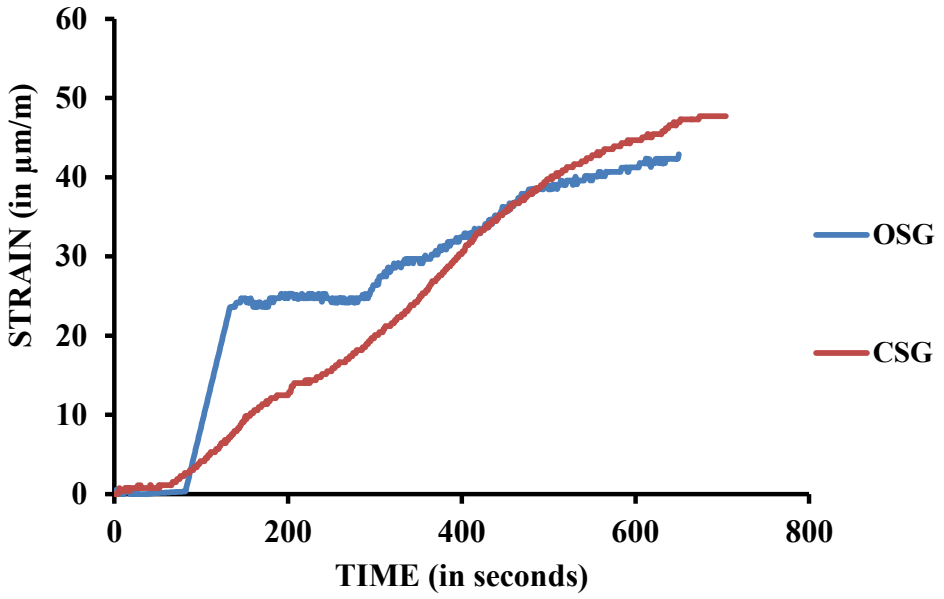

Fig.4. 16 Strain vs. Time curve for beam B2-50S

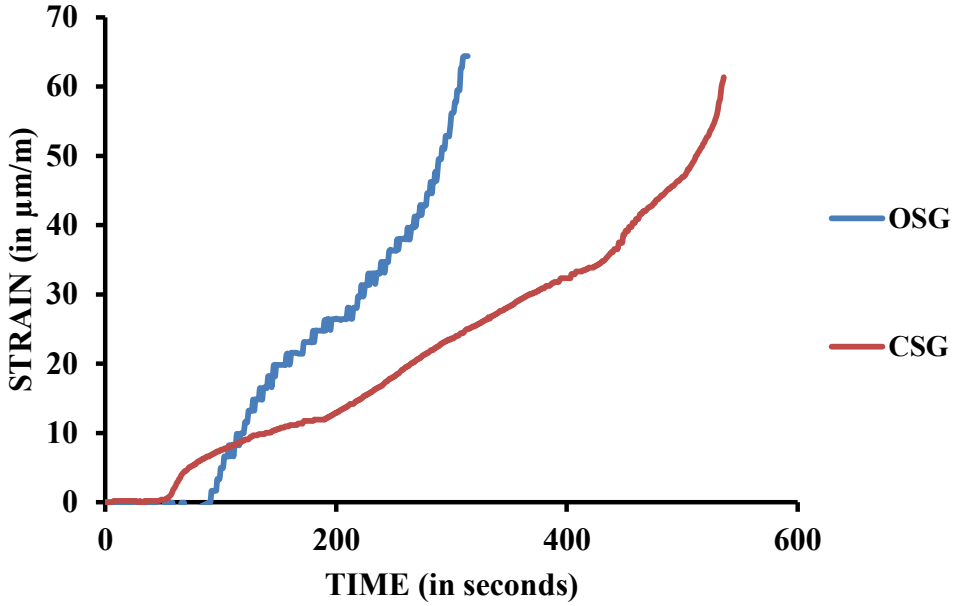

Fig.4. 17 Strain vs. Time curve for beam B2-70S

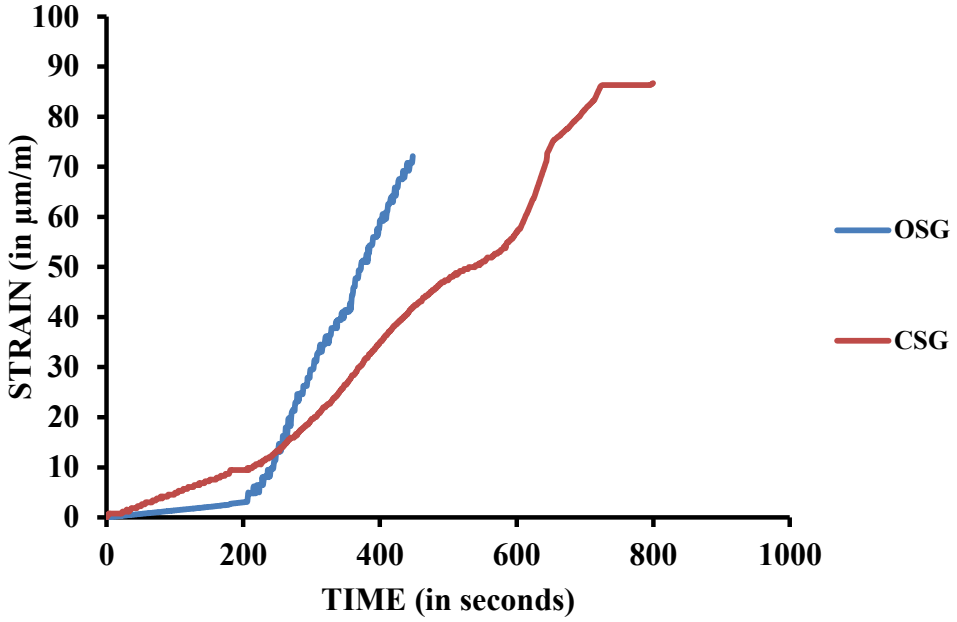

Fig.4. 18 Strain vs. Time curve for beam B3-50S

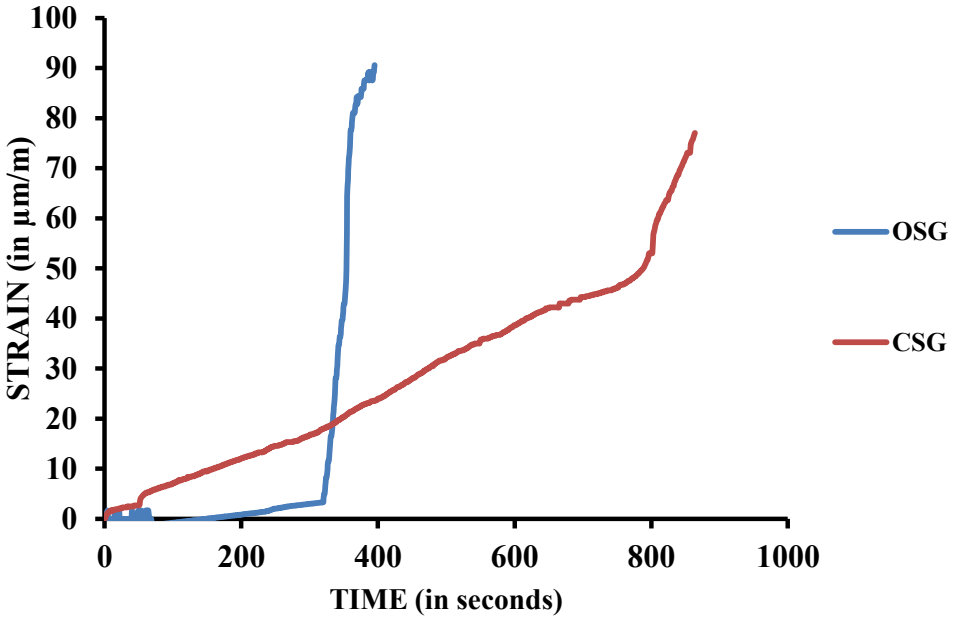

Fig.4. 19 Strain vs. Time curve for B3-70S

CONCLUSIONS

- Fiber optical sensors can become the biggest ally of the civil engineers in monitoring the health of the structures as their applications are numerous. They can be used as sensors which provide continuous, fast stream of data, depending upon the user's choice.

- With FBG fiber optical sensors one can monitor the health statically as well as dynamically as along with strain, displacement, acceleration sensors are also available which can know the accelerations as well.

- The data sent by the FOS is very high so enough electronic storage space should be available for the data stored by the data acquisition system.

- FBG sensors are an excellent replacement for conventional LVDT's and electrical strain gages. Though strain sensors didn't performed well on the surface coated with GFRP but on normal concrete (CB21, CB31 etc.) they performed well, in sync to each other. The behavior of strain sensor was observed to be change when mounted on GFRP strengthened beams as earlier OSG was giving higher values for longer time when connected to bare RC beam while CSG gave higher values for longer time when they were connected to GFRP strengthened beam. Also, optical strain gage pasted on a plate can be used again and again till the plate gets deflected. But work is needed to find an appropriate adhesive which can stick the plates to the materials like GFRP as well and maintain its reusability.

- GFRP is a very highly suited choice for strengthening of beams. Though the beams were damaged upto 50% and 70%, due to strengthening by GFRP their original load carrying capacity was restored i.e. for mix-proportion-1 it gave an increase of 3.77% and 2.20%, 1.29% and 6.02% increase in strength for 50% damaged beams, and 70% damaged beams respectively. Also, an observation to be noted here is that the failure of GFRP was considered as failure of beam though by the naked eye it seemed that the strengthened beams could have taken more load because the steel did not failed completely when the GFRP failed.

- GFRP also increased the initial stiffness to a commendable level, an average increase of 6 times the original value was observed but the secant stiffness was observed to fall down by an average of 0.2 times the original value. The other properties like deflection ductility and energy ductility were improved for the strengthened beams.

- The strengthening by GFRP was successful as it leads to the improvement in natural frequency and damage index of the specimens too.

Future Scope of work

Though this study has addressed the basic questions like how will the fiber optical sensors behave when tested under static continuous loading. But this may lead to a new set of questions like what if the load applied was not continuous , how will be the sensors behave when a step loading is applied to the beams? How to mount the sensors on GFRP or other smooth surfaces without compromising its reusability state as the conventional sensors can only be used once and if they are pasted on a separate plate they may get short-circuited or may give wrong results. After using it on linear surface like curved beams, how the fiber optical sensors will behave on a curved surface, this side could also be investigated. In end use of GFRP in other forms like bars etc, can also be studied.

REFERENCES

An, W., Saadatmanesh, H. and Ehsani, M.R., 1991. RC beams strengthened with FRP plates. II: Analysis and parametric study. Journal of Structural Engineering, 117(11), pp.3434-3455.

Baghiee, N., Esfahani, M.R. and Moslem, K., 2009. Studies on damage and FRP strengthening of reinforced concrete beams by vibration monitoring. Engineering Structures, 31(4), pp.875-893.

Bhutta, S. (1993). Analytical Modeling of Hybrid Composite Beams. M.S. Thesis, Dept. of Civil Engineering, Virginia Polytechnic Institute and State University, Blacksburg, VA.

Chan, T.H., Yu, L., Tam, H.Y., Ni, Y.Q., Liu, S.Y., Chung, W.H. and Cheng, L.K., 2006. Fiber Bragg grating sensors for structural health monitoring of Tsing Ma bridge: Background and experimental observation. Engineering structures, 28(5), pp.648-659.

Chung, W. and Kang, D., 2008. Full-scale test of a concrete box girder using FBG sensing system. Engineering Structures, 30(3), pp.643-652.

Clark, M.R., McCann, D.M. and Forde, M.C., 2003. Application of infrared thermography to the non-destructive testing of concrete and masonry bridges. Ndt & E International, 36(4), pp.265-275.

Costa, B.J.A. and Figueiras, J.A., 2012. Fiber optic based monitoring system applied to a centenary metallic arch bridge: Design and installation. Engineering Structures, 44, pp.271-280.

Inaudi, D. and Glisic, B., 2006, July. Distributed fiber optic strain and temperature sensing for structural health monitoring. In Proceedings of the Third International Conference on Bridge Maintenance, Safety and Management, Porto, Portugal (pp. 16-19).

IS 383:1970 (Reaffirmed 1997), Specification for coarse and fine aggregates from natural sources for concrete (Second Revision), Bureau of Indian Standards, July 1993.

IS 456:2000, Plain & Reinforced Concrete –Code of Practice (Fourth Revision), Bureau of Indian Standards, July 2000.

IS 1489 (Part 1):1991 (Reaffirmed 2005), Portland –Pozzolana cement-Specification Part1 Fly ash based, Bureau of Indian Standards, March 1993

IS 4031:1996 (Reaffirmed 2005), Method of Physical tests for hydraulic cement, Bureau of Indian Standards, 1996

IS 10262:2009, Cement mix proportioning - guidelines (First Revision), Bureau of Indian Standards, 2009.

Kanwar, V.S., Singh, R.P., Kwatra, N. and Aggarwal, P., 2016. Monitoring of RCC structures affected by earthquakes. Geomatics, Natural Hazards and Risk, 7(1), pp.37-64.

Kister, G., Winter, D., Gebremichael, Y.M., Leighton, J., Badcock, R.A., Tester, P.D., Krishnamurthy, S., Boyle, W.J.O., Grattan, K.T.V. and Fernando, G.F., 2007. Methodology and integrity monitoring of foundation concrete piles using Bragg grating optical fibre sensors. Engineering Structures, 29(9), pp.2048-2055.

Kim, J.T., Park, J.H. and Lee, B.J., 2007. Vibration-based damage monitoring in model plate-girder bridges under uncertain temperature conditions. Engineering Structures, 29(7), pp.1354-1365.

Kuang, K.S.C., Cantwell, W.J. and Thomas, C., 2003. Crack detection and vertical deflection monitoring in concrete beams using plastic optical fibre sensors. Measurement Science and Technology, 14(2), p.205.

Lau, K.T., Yuan, L., Zhou, L.M., Wu, J. and Woo, C.H., 2001. Strain monitoring in FRP laminates and concrete beams using FBG sensors. Composite structures, 51(1), pp.9-20.

Li, A., Assih, J. and Delmas, Y., 2001. Shear strengthening of RC beams with externally bonded CFRP sheets. Journal of Structural Engineering, 127(4), pp.374-380.

Li, H.N., Li, D.S. and Song, G.B., 2004. Recent applications of fiber optic sensors to health monitoring in civil engineering. Engineering structures, 26(11), pp.1647-1657.

Maia, N.M.M., Silva, J.M.M., Almas, E.A.M. and Sampaio, R.P.C., 2003. Damage detection in structures: from mode shape to frequency response function methods. Mechanical systems and signal processing, 17(3), pp.489-498.

McCann, D.M. and Forde, M.C., 2001. Review of NDT methods in the assessment of concrete and masonry structures. Ndt & E International, 34(2), pp.71-84.

Meda, A., Minelli, F. and Plizzari, G.A., 2012. Flexural behaviour of RC beams in fibre reinforced concrete. Composites Part B: Engineering, 43(8), pp.2930-2937.

Rehman, S.K.U., Ibrahim, Z., Memon, S.A. and Jameel, M., 2016. Nondestructive test methods for concrete bridges: A review. Construction and Building Materials, 107, pp.58-86

Ritchie, P.A., Thomas, D.A., Lu, L.W. and Connelly, G.M., 1990. External reinforcement of concrete beams using fiber-reinforced plastics.

Rhazi, J., 2000. NDT in civil engineering: the case of concrete bridge decks. CSNDT JOURNAL, 21(5), pp.18-25.

Rodrigues, C., Félix, C., Lage, A. and Figueiras, J., 2010. Development of a long-term monitoring system based on FBG sensors applied to concrete bridges. Engineering Structures, 32(8), pp.1993-2002.

Saadatmanesh, H. and Ehsani, M.R., 1991. RC beams strengthened with GFRP plates. I: Experimental study. Journal of structural engineering, 117(11), pp.3417-3433.

Salawu, O.S., 1997. Detection of structural damage through changes in frequency: a review. Engineering structures, 19(9), pp.718-723.

Shiotani, T., Aggelis, D.G. and Makishima, O., 2007. Global monitoring of concrete bridge using acoustic emission. Journal of acoustic emission, 25, pp.308-315.

Surre, F., Scott, R.H., Banerji, P., Basheer, P.A.M., Sun, T. and Grattan, K.T., 2012. Study of reliability of fibre Bragg grating fibre optic strain sensors for field-test applications. Sensors and Actuators A: Physical, 185, pp.8-16.

Tavares, D.H., Giongo, J.S. and Paultre, P., 2008. Behavior of reinforced concrete beams reinforced with GFRP bars. Revista IBRACON de Estruturas e Materiais, 1(3), pp.285-295.

Thalapil, J. and Maiti, S.K., 2014. Detection of longitudinal cracks in long and short beams using changes in natural frequencies. International Journal of mechanical sciences, 83, pp.38-47.

Triantafillou, T.C., 1998. Shear strengthening of reinforced concrete beams using epoxy-bonded FRP composites. Structural Journal, 95(2), pp.107-115.

Udd, E., 2017, June. Fiber optic smart structures. In Critical Review Collection (pp. 102660F-102660F). International Society for Optics and Photonics.

Uttamchandani, D., Culshaw, B., Overington, M.S., Parsey, M., Facchini, M. and Thévenaz, L., 1999. Distributed optical fibre sensing in synthetic fibre ropes and

cables. In 13th International Conference on Optical Fiber Sensors (No. THEVE-CONF-1999-001, pp. 8-11). Society of Photo-Optical Instrumentation Engineers.

Wegian, F.M. and Almottiri, F.A., Performance of Embedded Fiber Optic Sensors in Composite Structures.

APPENDIX-A

FRF GRAPHS OBTAINED FROM VIBRATION MONITORING OF BEAMS

BEFORE ANY LOADING WAS APPLIED

B2-50

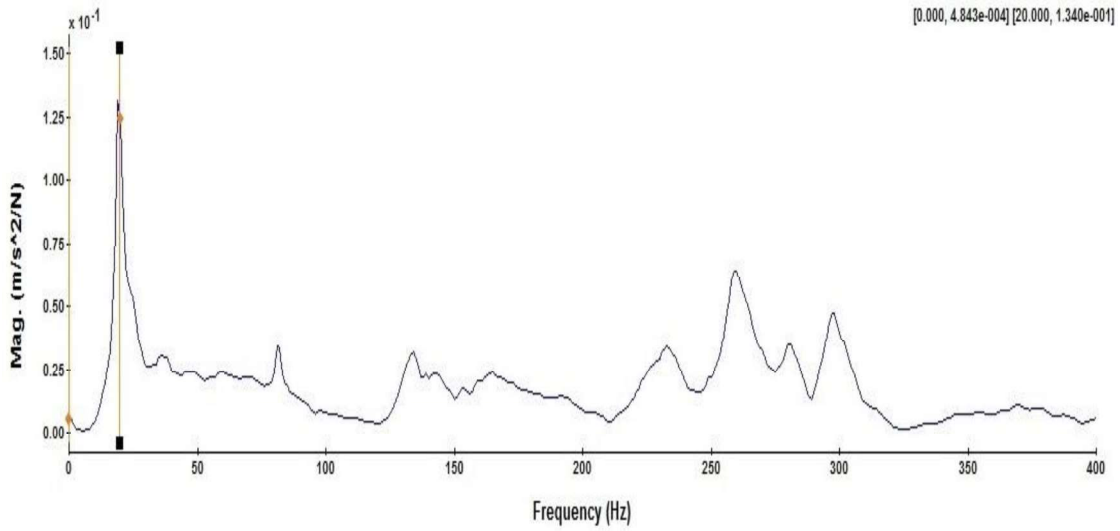

B2-70

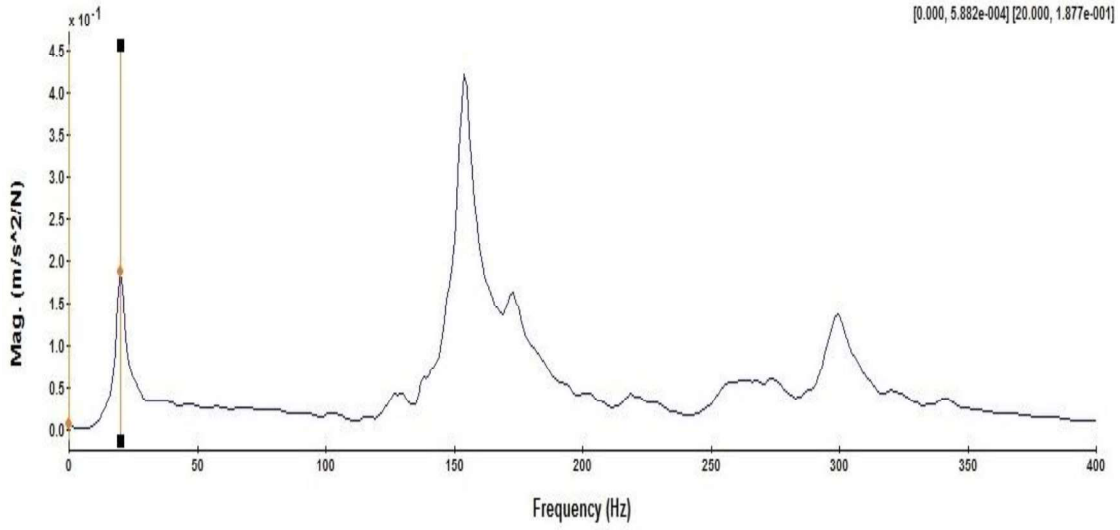

B3-50

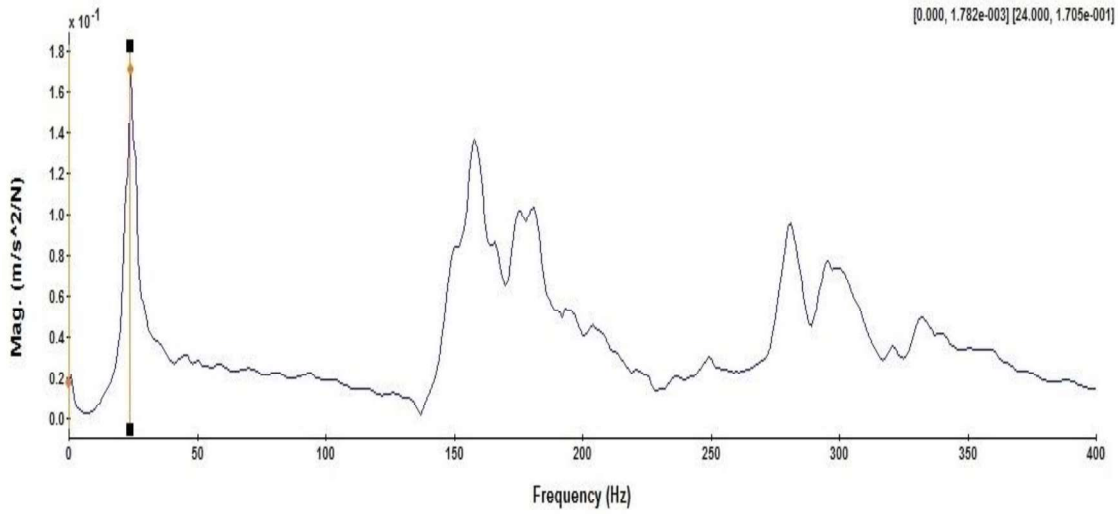
[0.000, 1.782e-003] [24.000, 1.705e-001]
x 10^-1
Mag. (m/s^2/N)
Frequency (Hz)

B3-70

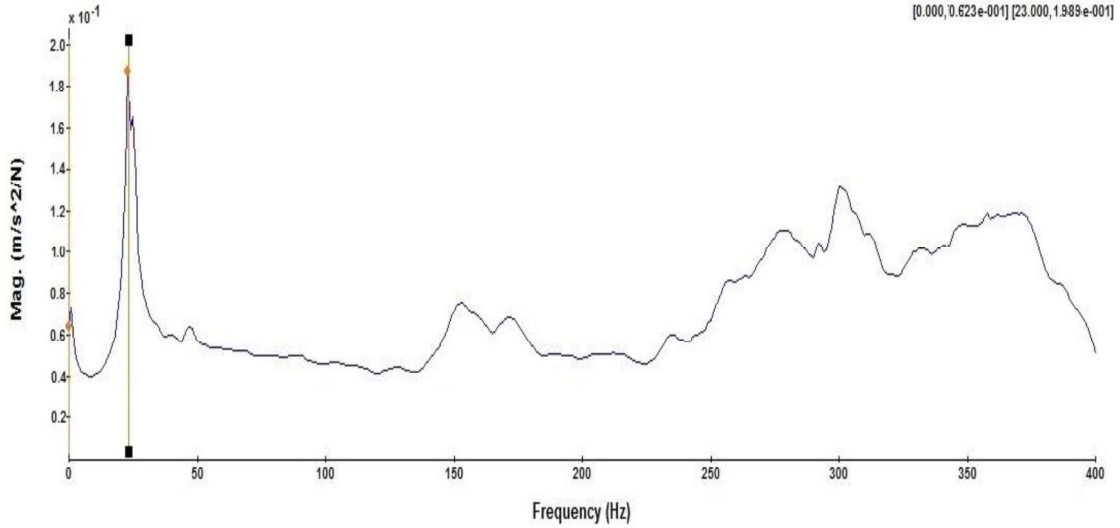
[0.000, 0.623e-001] [23.000, 1.989e-001]
x 10^-1
Mag. (m/s^2/N)
Frequency (Hz)

AFTER PRE-DAMAGING BEAMS BY 50% & 70% OF LOAD

B2-50

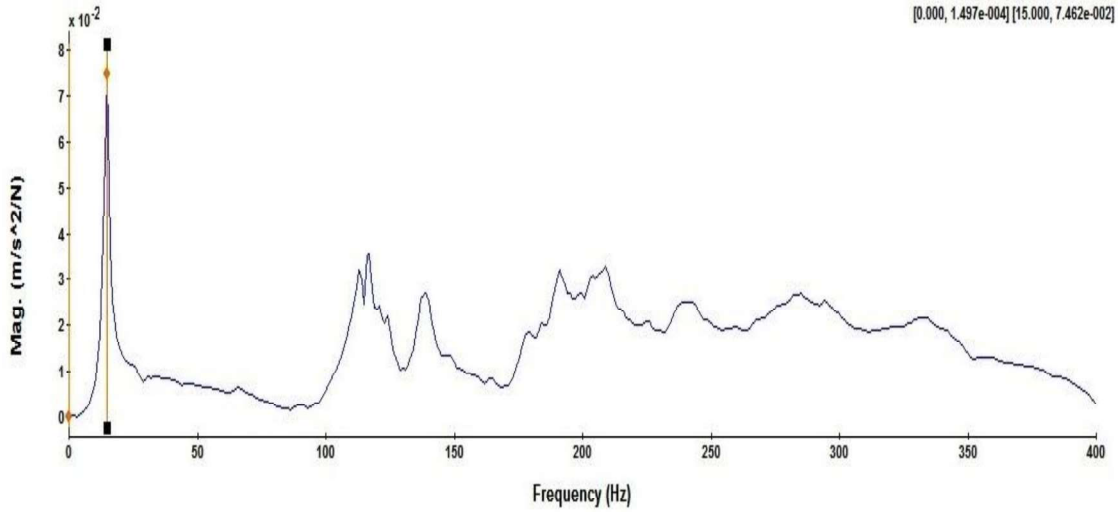

B2-70

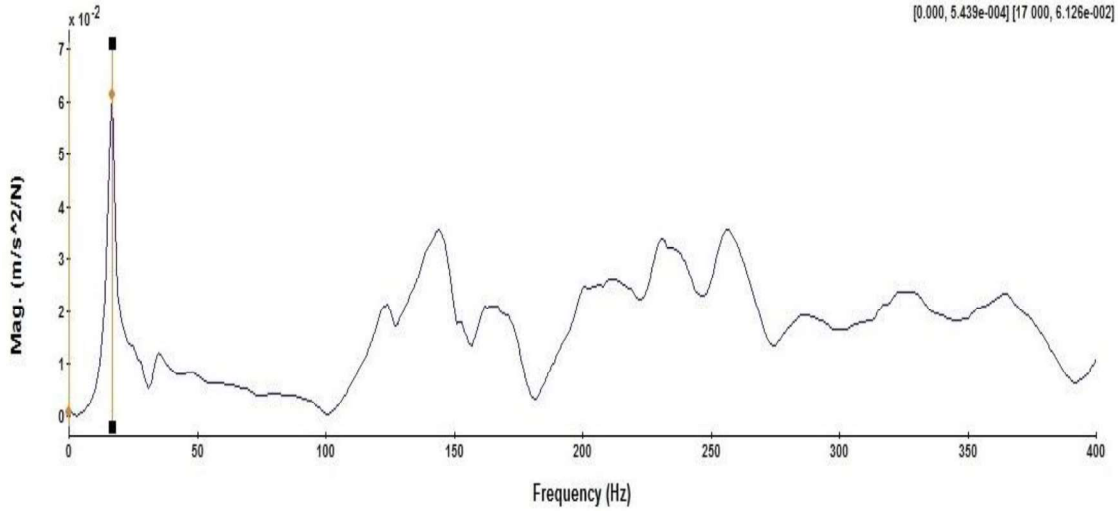

B3-50

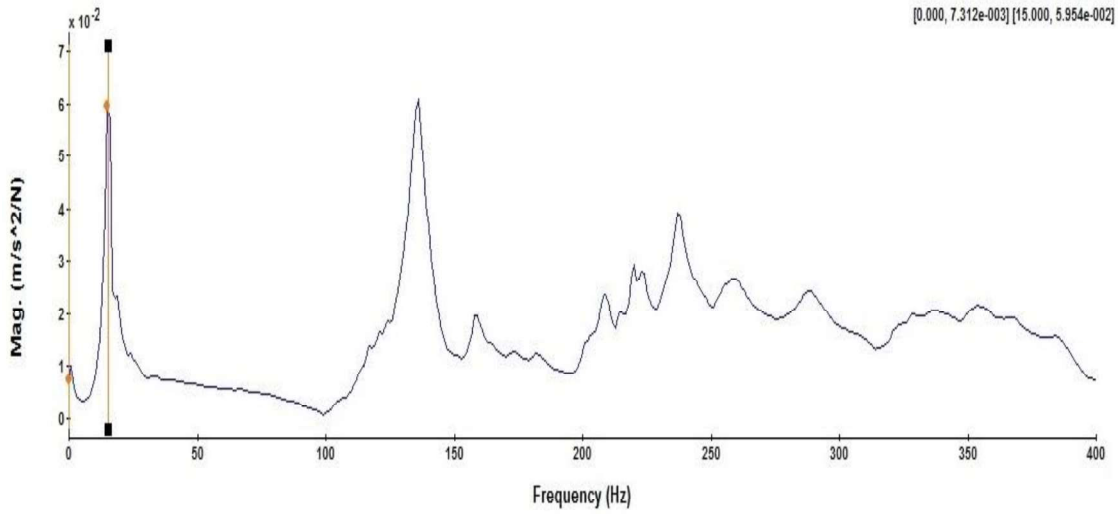
[0.000, 7.312e-003] [15.000, 5.954e-002]
x 10^-2
Mag. (m/s^2/N)
Frequency (Hz)

B3-70

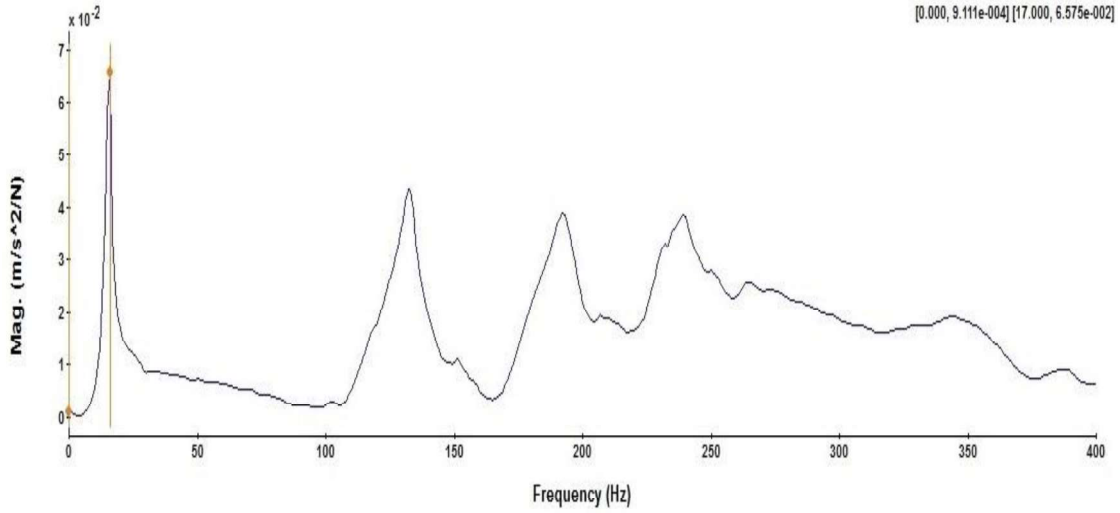
[0.000, 9.111e-004] [17.000, 6.575e-002]
x 10^-2
Mag. (m/s^2/N)
Frequency (Hz)

AFTER BEAMS WERE STRENGTHENED BY GFRP

B2-50S

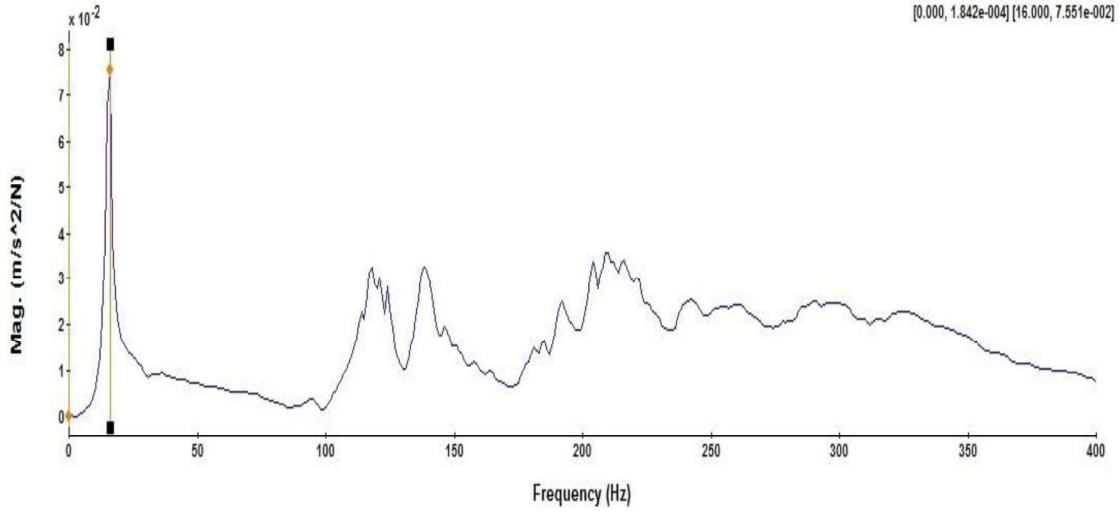

B2-70S

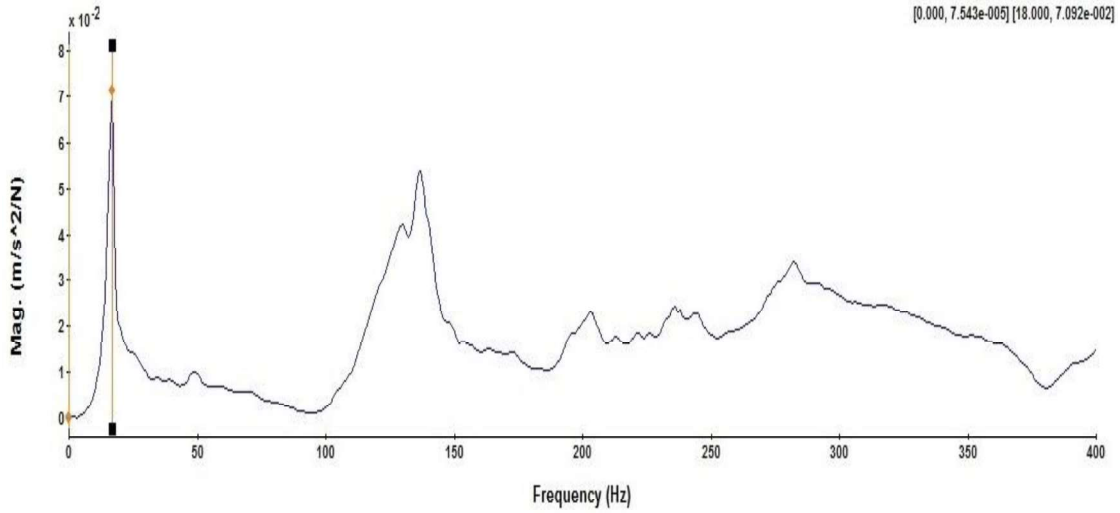

B3-50S

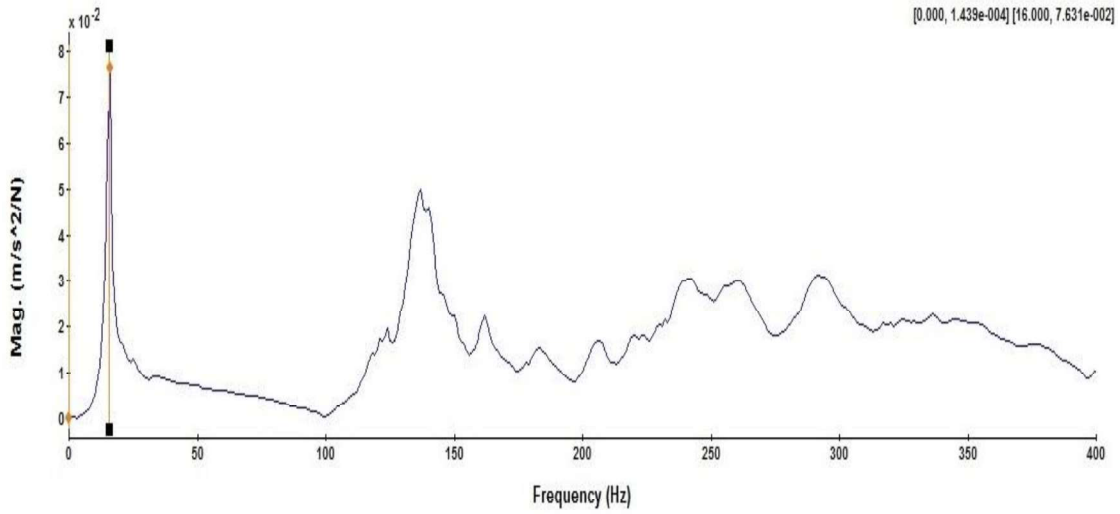
[0.000, 1.439e-004] [16.000, 7.631e-002]
x 10^-2
Mag. (m/s^2/N)
Frequency (Hz)

B3-70S

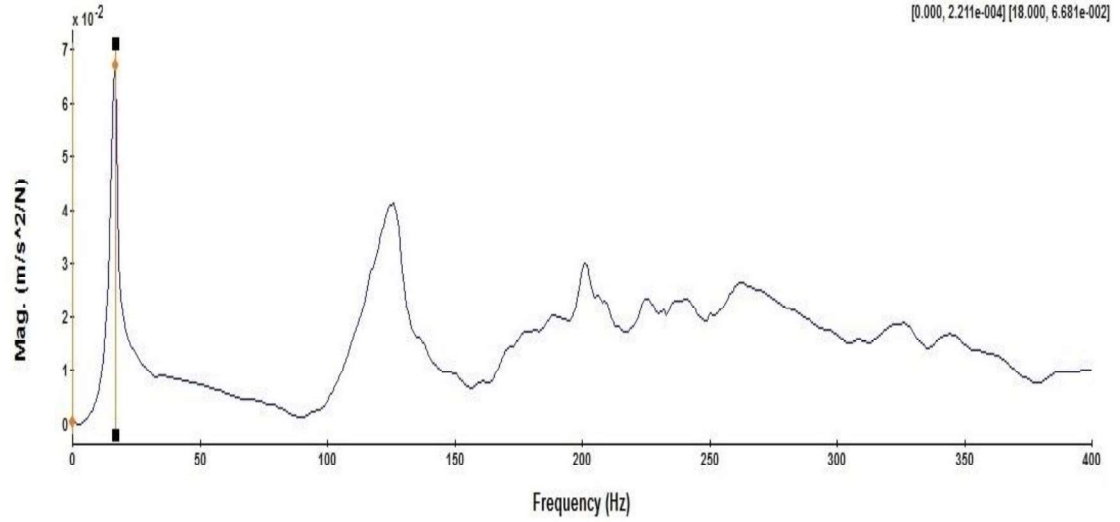
[0.000, 2.211e-004] [18.000, 6.681e-002]
x 10^-2
Mag. (m/s^2/N)
Frequency (Hz)